Risk Management of Cascading Failure in Composite Reliability of a Deregulated Power System with Microgrids

Quan Chen

Dissertation submitted to the faculty of the Virginia Polytechnic Institute and State University in partial fulfillment of the requirements for the degree of

Doctor of Philosophy
In
Electrical Engineering

Dr. Lamine M. Mili,	Chair
Dr. Virgilio A. Centeno,	Member
Dr. Cansin Yaman Evrenosoglu,	Member
Dr. Sandeep K. Shukla,	Member
Dr. Michael R. von Spakovsky,	Member

December 9th, 2013
Falls Church, Virginia

Keywords: Reliability Evaluation, Cascading Failure, Microgrid, Monte Carlo, Variance Reduction Technique, Optimal Placement

Risk Management of Cascading Failure in Composite Reliability of a Deregulated Power System with Microgrids

Quan Chen

ABSTRACT

Due to power system deregulations, transmission expansion not keeping up with the load growth, and higher frequency of natural hazards resulting from climate change, major blackouts are becoming more frequent and are spreading over larger regions, entailing higher losses and costs to the economy and the society of many countries in the world. Large-scale blackouts typically result from cascading failure originating from a local event, as typified by the 2003 U.S.-Canada blackout. Their mitigation in power system planning calls for the development of methods and algorithms that assess the risk of cascading failures due to relay over-tripping, short-circuits induced by overgrown vegetation, voltage sags, line and transformer overloading, transient instabilities, voltage collapse, to cite a few. How to control the economic losses of blackouts is gaining a lot of attention among power researchers.

In this research work, we develop new Monte Carlo methods and algorithms that assess and manage the risk of cascading failure in composite reliability of deregulated power systems. To reduce the large computational burden involved by the simulations, we make use of importance sampling techniques utilizing the Weibull distribution when modeling power generator outages. Another computing time reduction is achieved by applying importance sampling together with antithetic variates. It is shown that both methods noticeably reduce the number of samples that need to be investigated while maintaining the accuracy of the results at a desirable level.

With the advent of microgrids, the assessment of their benefits in power systems is becoming a prominent research topic. In this research work, we investigate their potential positive impact on power system reliability while performing an optimal coordination among three energy sources within microgrids, namely renewable energy conversion, energy storage and micro-turbine generation. This coordination is modeled when applying sequential Monte Carlo simulations, which seek the best placement and sizing of microgrids in composite reliability of a deregulated power system that minimize the risk of cascading failure leading to blackouts subject to fixed investment budget. The performance of the approach is evaluated on the Roy Billinton Test System (RBTS) and

the IEEE Reliability Test System (RTS). Simulation results show that in both power systems, microgrids contribute to the improvement of system reliability and the decrease of the risk of cascading failure.

Acknowledgement

I really enjoy this moment. After more than four-year journey, finally I have arrived the point when I can look back and write down some thankful words before Thanksgiving Day.

First and foremost, I would like to express my greatest gratitude to my adviser, Dr. Lamine Mili, who is not only my mentor but friend. His enlightening vision and constant patience dragged me out of confusion and depression during my bad times. His support and encouragement enables me to keep confident, no matter how tough my situation might be. I could not imagine how I would get through these without his invaluable support. I also appreciate his recommendations and suggestions for my career development. He was and remains my best role model of an inspirational, enthusiasm, disciplined, and humorous scientist and mentor. What I have learned from him, including academics and living attitudes, will benefit me for the rest of my life. I am forever grateful. Thank you, Dr. Mili!

I am thankful to all the members of my Ph.D. committee, namely Dr. Yaman Evrenosoglu, Dr. Sandeep Shukla, Dr. Virgilio Centeno, and Dr. Michael von Spakovsky, for their encouraging and constructive feedback. I would like to give special thanks to Dr. von Spakovsky, who carefully corrected my English writing mistakes in my Preliminary Report. I learned the importance of the English writing ability and kept practicing writing skills. Also thank to Dr. Mili, now I can feel the improvement of my written English.
Next I would like to thank my dear friends at Northern Virginia Center (NVC). Because of them, the experience at NVC becomes a joyful journey. We share. Their concerns keep me away from loneliness.

Finally and more deeply, I would like to delicate my dissertation to my parents. Your unconditional love and complete support carry me along the way. I know I always have you to count on when times are rough. Thank you with all my heart and soul. There are no words can express how much I love you.

Contents

List of Figures

List of Tables

Chapter 1

Introduction

1.1 Background

As power system loading increases, large blackouts resulting from cascading outages become more likely. Although massive blackouts are rare events, they are extremely costly to society with estimates of direct costs that typically amount to several billions of dollars. As an example, let us consider the 2003 U.S.-Canada blackout. The total cost estimates in the United States range between $4 billion to $10 billion U.S. dollars. Gross domestic product decreased 0.7% in August in Canada; there was a net loss of 18.9 million work hours, and manufacturing shipments in Ontario decreased $2.3 billion (Canadian dollars) [1]. There are also indirect costs such as social unrest and the cost of the impact of the propagation of failures into other infrastructures such as communications, water supply, natural gas, and transportation. The importance of electric power to our society motivates continued attention to maintaining power system stability and reliability and developing new methods to manage the risks of cascading failures.

1.1.1 Modeling Challenges of Cascading Failure

The IEEE PES CAMS Task Force report [2] defines cascading failure as "a sequence of dependent failures of individual components that successively weakens the power system". In this report [2], a power system is viewed as "including not only the many physical components but also the software, procedures, people, and organizations that design, operate, and regulate the power system". While the initial failure can be seen as a random event, a causal link exists between the subsequent events afterwards. The characteristic of this link varies. In some cases it is "electrical" (*e.g.*, overloading). In some other cases, the reaction of control or protection devices (both hardware and software) to previous events may lead to the next one. Moreover, human operators that take inappropriate actions or fail to take action either due to a lack of training or experience, or a lack of situational awareness might be another type of such links. These causal links are usually considered as being "hidden" in the sense that they do not emerge until some event exposes their existence. For example, hidden failures in protection

relays might disconnect healthy components unnecessarily when there is a fault. In the 2003 U.S.-Canada blackout, the reasons for some of the hidden failures have not been identified so far.

In composite power transmission system planning and operation, an N-1 contingency analysis [74] is widely used. In some stringent cases, an N-2 security analysis [74] is executed. However, it is implemented not via an exhaustive search but rather via a partial assessment of the system that covers a small portion of the transmission work. But neither an N-1 nor an N-2 security analysis is enough for assessing the impact of cascading failure. An N-k security analysis for k>1 is considered as being improbable to achieve due to the huge number of cases that need to be investigated. Although the dependence between successive events in a cascading failure makes the number of cases smaller than a random (*i.e.*, independent) tripping of k out N components of the system, the sampling size is still prohibitively large because of the diversity of failures and the many different mechanisms by which failures propagate. There are also a variety of modeling requirements and timescales (milliseconds for electromechanical effects and tens of minutes for voltage support and thermal heating). Combinations of several types of failures and interactions can typically occur in large blackouts, including cascading overloads, failures of protection devices, transient instability, forced or unforced initiating failures, lack of reactive power and voltage collapse, unavailability of a program for power system security monitoring and analysis such as a state estimator and contingency analysis, lack of situational awareness, communication mistakes, and operational errors. Most work in power system cascading failures has so far focused on only one of these aspects. While these investigations have made advances in understanding and modeling each aspect, they do not provide a framework for understanding the overall phenomenon.

1.1.2 Emergence of Microgrids

Power system planning is undergoing a transition towards probabilistic approaches due to, among other things, deregulation and interconnection of microgrids triggered by public concerns regarding rising electric energy costs, more frequent power outages, limited fossil fuel resources, and increasing environmental air and water pollution, to cite a few [3]. Microgrids, which are small-scale networks interconnecting distributed generation (DG), storage devices, loads and converters, are evolving thanks to technological advancements.

The benefits of microgrid integration on power system reliability include for example:

- controlling the voltage at the point of interconnection with the main grid;

- decreasing peak load demand in normal conditions and supplying reserve in abnormal conditions;
- reducing transmission losses and mitigating transmission overloading and congestions;
- providing flexible operation in both islanded mode and grid-connected mode.

In view of the foregoing benefits, we may say that interconnecting microgrids with a power system may lead to a reduction of the risk of cascading failure leading to blackouts. Our investigation will reveal under which conditions this risk reduction may occur.

1.2 Contributions

1.2.1 Development of two Speed-up Algorithms for Reliability Evaluation Simulation Involving Cascading Failure

A risk-based method for composite power system vulnerability evaluation to cascading failures via sequential Monte Carlo simulations is developed. Numerous scenarios with a feasible sampling size are considered so that the risk of cascading failure is reasonably estimated when achieving power system expansion. To decrease the computational burden, an importance sampling technique utilizing the Weibull distribution is applied to the generator outages. For further improvement, we propose another method combining importance sampling and antithetic variates together. This combined method is only applied to the generator outages, because the antithetic variates algorithm is not suited to the simulation of transmission line outages in the state sampling approach. It is shown that the importance sampling algorithm requires roughly one-third to one-half of the number of samples required by the conventional Monte Carlo method to reach a desired level of accuracy depending on the system under test, while the combined method decreases this ratio even further.

1.2.2 Assessing the Impacts of Microgrid Penetration on Composite Power System Reliability

The impacts of microgrids on composite power system reliability using sequential Monte Carlo simulations is analyzed. In these simulations, a search for an optimal coordination within microgrids is carried out. It involves various devices including renewable energy conversion, energy storage, and micro-turbine generation. The overall objective is to assess the risk of cascading failure due to relay overtripping, short-circuits induced by overgrown vegetation, voltage sags, line and transformer overloading, transient

instabilities, voltage collapse, to cite a few. It is shown that microgrids significantly improve system reliability and decrease the risk of cascading failure in multiple ways.

1.2.3 Development of an Optimization Method of Microgrid Placement and Sizing for System Reliability Enhancement

Upon completion of the Monte Carlo simulations of reliability evaluation on a microgrid-embedded system, a quadratic programming algorithm is executed. It provides a collection of optimal solutions of microgrid placement and sizing for various abnormal states of the system. By resorting to cluster analysis and the least-squares method, a single final solution is identified as representative of the largest cluster of candidates. To evaluate the proposed approach, two case studies are carried out on the Roy Billinton Test System (RBTS) and the IEEE Reliability Test System (RTS). Simulation results show that for both power systems, a small penetration of 5% of microgrids induces a significant improvement in system reliability while decreasing the risk of cascading failure.

1.3 Organization of the Dissertation

This dissertation is organized as follows. Chapter 2 provides a brief introduction about the 2003 U.S.-Canada blackout based on the official final report made by the U.S. - Canada Power System Outage Task Force. Chapter 3 illustrates the performances of variance reduction techniques in power system adequacy assessment. Chapter 4 describes the implementation of the importance sampling (IS) method and the importance sampling and antithetic variates (IS-AV) combined method on composite power system reliability evaluation. Chapter 5 is devoted to optimal placement and sizing of microgrids for reliability enhancement in a deregulated power system. Chapter 6 then depicts an agenda for future work.

Chapter 2

2003 U.S.-Canada blackout review

This chapter provides a literature review on the 2003 U.S.-Canada blackout. The first sub-section analyzes the sequence of events that resulted in this large-scaled blackout, while the second sub-section conducts a further discussion on what was learned about this outage.

2.1 General review of the blackout

On August 14, 2003, large portions of the Midwest and Northeast United States and Ontario, Canada, experienced an electric power blackout. There were an estimated 50 million people suffering from this outage with 61,800 megawatts (MW) of electric load loss. The blackout can be divided into two stages. The first stage started from normal operating conditions, then went into a period of abnormal but still potentially manageable conditions, and finally into an uncontrollable sequence of events in northern Ohio. The second stage is called the cascade stage in which the blackout spread in Ohio and then across the Northeast.

Let us analyze the initial stage first. The power system in northern Ohio was operating under normal condition, still normally serving all the energized loading in its area after the losses of the Eastlake 5 unit and Stuart-Atlanta 345-kV transmission line. However, their status was not updated by MISO's (Midwest Independent System Operator) state estimator as it was supposed to have been. Without an effective state estimator, MISO was unable to perform contingency analysis, which precludes them from realizing that the transmission line loadings were notably high and the system margin was getting very small. MISO's state estimator and contingency analysis had failed to solve successfully since 12:15 EDT due to a combination of human errors and computer failures. These functions were finally restored at 16:04 EDT, about two minutes before the start of the cascade. From 15:05 EDT to 15:42 EDT, three FirstEnergy (FE) 345-kV transmission lines in the Cleveland area tripped below their emergency rating due to overgrown trees. Their outages increased the loading on the remaining lines and decreased voltages on the rest of the system, pushing those lines into overload. The 138-kV transmission system

collapsed in Northern Ohio 29 minutes after the overloaded lines tripped one by one. The initial stage ended up with the failure of the Sammis-Star 345-kV transmission line.
Generally speaking, most large-scale blackouts start for different reasons, but when they grow into the cascade stage, there are many common characteristics among them. The loss of the Sammis-Star line due to a zone-3 impedance relay marked the turning point at which system problems in northeast Ohio initiated a cascading blackout across the northeast United States and Ontario. After that, thirteen 345-kV or 138-kV transmission lines in Ohio and Michigan tripped in 5 minutes by zone 2 or 3 relays, because the depressed voltages caused the line overloads to appear to the protective relays as a remote fault on the system. So the operation of zone 2 and 3 relays greatly expanded and accelerated the spread of the cascade. At the same time, the oscillation continued getting stronger; the voltages were also declining faster and the system was losing power plants. Since the link for northern Ohio to the south had been cut off, electricity moved along a giant loop through Pennsylvania and into New York and Ontario and then into Michigan via the remaining transmission path to serve the combined loads of Cleveland, Toledo, and Detroit. Thousands of events occurred on the grid between 16:10:36 EDT and 16:13 EDT due to automatic equipment operations. When it was over, several electrical islands formed in northeast U.S. and Canada, including Ohio, Michigan, Pennsylvania, New York, Vermont, Massachusetts, Connecticut, New Jersey and Ontario.

2.2 Discussion about the Blackout

As we see, the grid was split into the sections that experienced a blackout and those that recovered without further propagating the cascade. In the U.S. Midwest, as voltage levels declined many generators in the affected area were operating at maximum reactive power output before the blackout. This left the system little margin to deal with low voltage conditions, unable to ramp up more generators to higher reactive power output levels, so that little room to absorb any system “bumps” in voltage or frequency was available. In contrast, in the northeast—particularly in PJM, New York, and ISO-New England—operators were anticipating high power demands on the afternoon of August 14 and had already set up the system to maintain higher voltage levels and therefore had more reactive reserves on-line in anticipation of later afternoon needs. Thus, when the voltage and frequency swings began, these systems had reactive power readily available to help buffer their areas against potential voltage collapse without widespread generation trips.

The second discussion is about Under-Frequency and Under-Voltage Load-Shedding (UFLS & UVLS). The load shedding before the loss of the Sammis-Star line might have prevented the cascade and blackout. However, when large-scale dynamic oscillations were spreading throughout the northeast system in the cascade stage, they would have

made stabilization difficult and unlikely, even if the UFLS and generation had been perfectly balanced at any moment in time.

Thirdly, let us discuss why so many generators tripped in the blackout. According to [1], at least 265 power plants with more than 508 individual generating units shut down in the August 14 blackout. Within the overall cascade sequence, 29 (6%) generators tripped because of the generators' protective relays responding to overloaded transmission lines. Fifty more generators (10%) tripped as the islands formed, particularly due to changes in configuration, loss of synchronism, excitation system failures with some under-frequency and under-voltage. In the third phase of generator losses, 431 generators (84%) tripped after the islands formed, many at the same time as under-frequency load-shedding was occurring. Some generators became completely removed from all the loads. When there was no load to be served the power plant shut down in response to over-speed and/or over-voltage protection schemes. Others were overwhelmed because they were among a few power plants within an electrical island and were suddenly called on to serve huge customer loads so the imbalance caused them to trip on under-frequency and/or under-voltage protection.

The fourth issue in the discussion concerns the transmission line failures. In the initial stage of the 2003 blackout, three 345-kV transmission lines in the Cleveland area tripped successively below their emergency rating due to overgrown trees. Their relative outages were some of the core reasons triggering the domino events which were not controllable for the system operator, pushing the power system towards the critical edge of voltage collapse. Actually, the vegetation issue is more likely to appear in the summer since the higher ambient temperature increases the overhead conductor sag. Moreover, the misoperation of impedance relays, especially zone 3 and zone 2 impedance relays, played another important role in the cascading failures. This problem cannot be simply solved by adjusting the relay settings or improving the relay accuracy because the voltage decline is inevitable during system degradation.

Finally, high voltage DC (HVDC) transmission is able to block the spread of the cascade. The Quebec system in Canada, which survived in this large-scale blackout, is tied to the remainder of the Eastern Interconnection via HVDC lines instead of AC transmission lines. The frequency swings were shielded by DC links, so that dynamic oscillations could not affect the Quebec system. Therefore, segmentation by means of DC connections has been suggested to be used to expand transfer capability.

Chapter 3

Monte Carlo and Variance Reduction Techniques in Power System Adequacy Assessment

3.1 Monte Carlo and Variance Reduction Methods

As it has been discussed in Chapter 1, the evaluation of cascading failure probability is a combinatorial problem. Generally speaking, there are two main categories of evaluation techniques: analytical and computational methods. Analytical methods represent the system by analytical models and derive the responses of these models using mathematical solutions. On the other hand, Monte Carlo simulation methods estimate the responses by simulating the actual random behavior of the system. These methods, therefore, treat the problem as a series of scenarios. Since many types of cases might occur in cascading failure, Monte Carlo methods are often preferred.

Monte Carlo method can be defined as any method which solves a problem by generating suitable random numbers and observing that fraction of the numbers obeying some property or properties [4]. Despite the many advantages of Monte Carlo methods in reliability analysis of large-scale systems, their disadvantages must not be overlooked. One of the most significant disadvantages of the Monte Carlo method is its large computing burden due to the large number of samplings that need to be processed to achieve a desired level of accuracy.

To circumvent that weakness, variance reduction methods may be used. These methods may decrease the number of Monte Carlo trials while maintaining a desired level of accuracy by reducing the variance of the sample-mean estimator under study based on known information about the problem. There are several well-known variance reduction techniques proposed in the literature. The most popular ones are importance sampling (IS), control variates (CV), stratified sampling (SS), antithetic variates (AV) and dagger sampling (DS), some of which will be introduced into power system adequacy assessment as follows.

3.2 Hierarchy and Indices of Power System Reliability

In general terms, power system can be divided into three functional components, namely generation, transmission, and distribution subsystems. According to this functional decomposition, three hierarchical levels of reliability evaluation can be performed. Hierarchical Level 1 (HL1) is concerned only with generation; Hierarchical Level 2 (HL2), which is also called composite power system, deals with both generation and transmission while HL3 includes all three functional components in an assessment of consumer load point adequacy. HL3 studies are not usually conducted directly in a practical system due to the enormity of the problem. The reliability study on HL2 is discussed in the next two chapters. HL1 studies mainly focus on adequacy assessment, which is utilized to illustrate the application of the variance reduction techniques in this chapter.

There are different indices for each HL. The typical adequacy indices in HL1 studies like LOLE, LOEE, and LOLF have been widely used by power utilities. Here are the definitions used in Monte Carlo simulations. Note that N denotes the number of trials.

LOLE – loss of load expectation

$$LOLE = \frac{1}{N}\sum_{i=1}^{N} LLD_i \tag{3-1}$$

LLD – loss of load duration.

LOEE – loss of energy expectation

$$LOEE = \frac{1}{N}\sum_{i=1}^{N} ENS_i \tag{3-2}$$

ENS – energy not supplied.

LOLF – loss of load frequency

$$LOLF = \frac{1}{N}\sum_{i=1}^{N} LLO_i \tag{3-3}$$

LLO – loss of load occurrence.

Variance reduction techniques exploit the known information that is available about the problem. Different variance reduction techniques are chosen according to what kind of information we know. Three types of such techniques are implemented in the following sections. For simplicity, all the components have only two states in these simulations – normal state and failure state.

Generally speaking, there are three different simulation approaches in reliability evaluation [4]. First, in the state sampling approach, a uniformly distributed random variable is generated to decide whether the component state is in failure mode or not. That is, if the random variable is larger than the failure probability, the component is in a normal state; otherwise, it fails. The system state is the combination of all component states. Second, the state duration sampling approach uses component state duration distribution functions. In a two-state component representation, these are operating and repair state duration distribution functions, which are usually assumed to be exponentially distributed. Finally, in the state transition sampling approach, there is a transition probability that represents the probability of the departure from the previous state to the present state in the time domain. Most of the related applications are based on Markov chains [4] where the transition probability is usually a fixed number, which is not the case in a typical process of cascading failures. This approach will not be implemented in the simulations below.

3.3 Importance Sampling

3.3.1 Introduction

Suppose one has a multiple dimensional integral given by

$$I = \int g(x)dx, \qquad x \in D \subset R^n \tag{3-4}$$

Applying the importance sampling technique, the integral (3-4) can be represent as

$$I = \int \frac{g(x)}{f_X(x)} f_X(x)dx = E\left[\frac{g(X)}{f_X(X)}\right] \tag{3-5}$$

where X is a set of random variables with probability distribution function (p.d.f.) $f_X(x)$, which satisfies $f_X(x) \geq 0$ and $\int_D f_X(x)dx = 1$.

An unbiased estimator is represent as

$$\hat{I} = \frac{1}{N}\sum_{i=1}^{N} \frac{g(X_i)}{f_X(X_i)} \tag{3-6}$$

As said above, if the simulation number N is fixed, reducing the variance of $\hat{I}$ is equivalent to reducing the variance of $\xi = \frac{g(X)}{f_X(X)}$. Now it will be shown how to get a proper distribution of a random variable, X, in order to minimize the $Var(\xi)$.

It can be proven that if $g(x) > 0$, then the optimal p.d.f. is

$$f_X(x) = \frac{g(x)}{I} \tag{3-7}$$

and the $Var(\xi) = 0$.

The detailed proof can be found in Rubinstein's book [4]. Next, an intuitive explanation of Eq. (3-7) is given.

To get the best performance, that is $Var(\xi) = 0$. ξ is expressed as

$$\xi = \frac{g(X)}{f_X(X)} = \alpha, \tag{3-8}$$

where α is a constant.

If one can find $f_X(x)$ such that $f_X(x) = \frac{g(x)}{\alpha}$, Eq. (3-8) is satisfied.

As is known, $f_X(x) \geq 0$ and $\int_D f_X(x)dx = 1$ so that $g(x) > 0$, and $\int_D \frac{g(x)}{\alpha}dx = 1$. Then

$$\alpha = \int_D g(x) = I. \tag{3-9}$$

Therefore, the optimal p.d.f. is Eq. (3-7).

However, the value of I is unknown, so a distribution function "similar" to $g(x)$ is simply postulated if is known the latter.

In sum, the importance sampling method samples random variates with the distribution of the estimation target $g(x)$ if known a priori, instead of the original distribution of x.

3.3.2 Importance Sampling in Adequacy Assessment

The exponential failure model for the chronological state change of generators has been widely used in reliability analysis. Estimating the mean-time-to-failure, which is denoted as I, yields

$$I = MTTF = \int_0^\infty x f_e(x)dx, \tag{3-10}$$

where $f_e(x)$ is the p.d.f. of the exponential distribution with the parameter λ or μ. A p.d.f. is then chosen, which is similar to the scaled shape of $g(x) = xf_e(x)$, for example, the Rayleigh distribution (Fig. 3-1). Note that the Rayleigh parameter value is usually obtained using a least-squares algorithm.

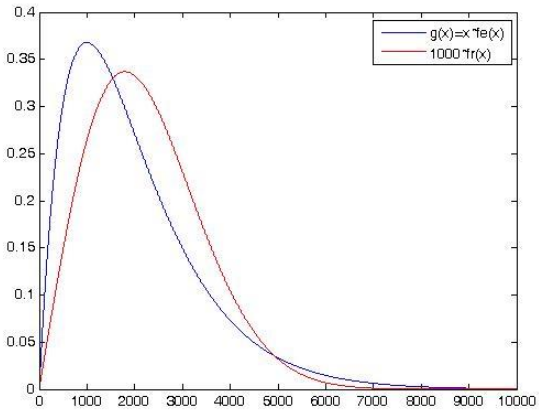

Fig. 3-1 Comparison of $g(x)$ and the scaled p.d.f of the Raleigh distribution $f_r(x)$ with $b = 1800$.

Applying the importance sampling method results in

$$I = \int_0^\infty \frac{x f_e(x)}{f_r(x)} f_r(x) dx \, . \tag{3-11}$$

A least-squares estimator of I is expressed as

$$\hat{I} = \sum_{i=1}^{N} \frac{X_i f_e(X_i)}{f_r(X_i)} \, . \tag{3-12}$$

The performance of the importance sampling algorithm for a particular case is illustrated in the next section.

3.3.3 Case Study

The IEEE one-area RTS has 9 types of 32 generating units ranging from 12 MW to 400 MW. The annual load curve consists of $52 \times 7 \times 24 = 8736$ hourly load points. The load data (Fig. 3-2) for a typical sample year and generating unit data can be found in [4]. Here three types of generating units that are associated with the three largest exponential parameters (2940, 1980 and 1960) are deleted. The reason is that in our 2500 years of simulation, the component states are not continuous year by year. The initial component states of each year are always normal. So the large exponential parameters, which in fact are MTTFs, have too large a value compared to the number of hourly points in each year, yielding 8736 points if the initial state assumption error is ignored.

Figs. 3-3 – 3-5 show that the estimators of the three reliability indices, namely LOLE, LOEE and LOLF, tend to converge to some value as the simulation number goes up. We

may also find that the variance of the importance sampling estimator is smaller than the variance of the conventional Monte Carlo method (Figs. 3-6 – 3-8).

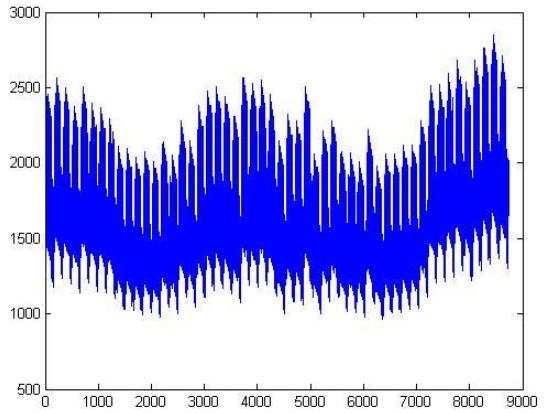

Fig. 3-2 Load of a typical sample year over 8736 hourly points.

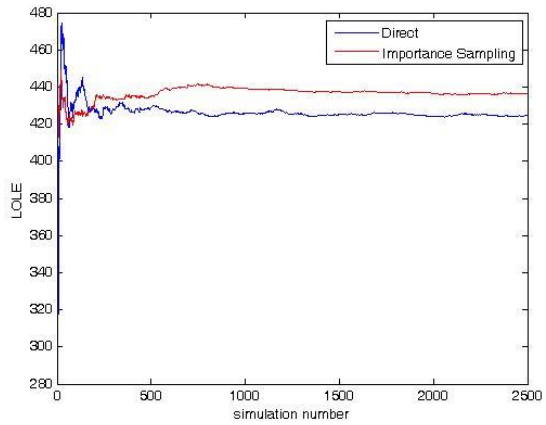

Fig. 3-3 LOLE comparison between the conventional and importance sampling algorithms.

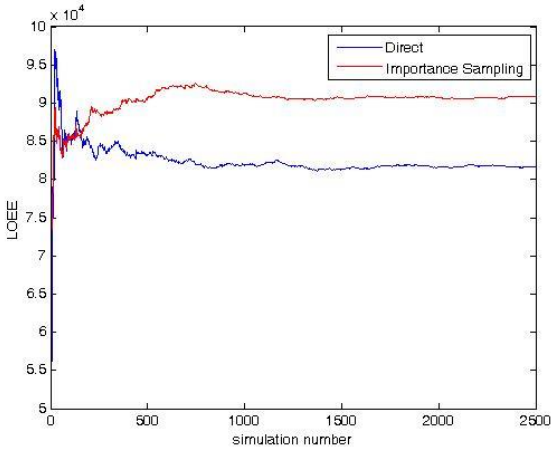

Fig. 3-4 LOEE comparison between the conventional and importance sampling algorithms.

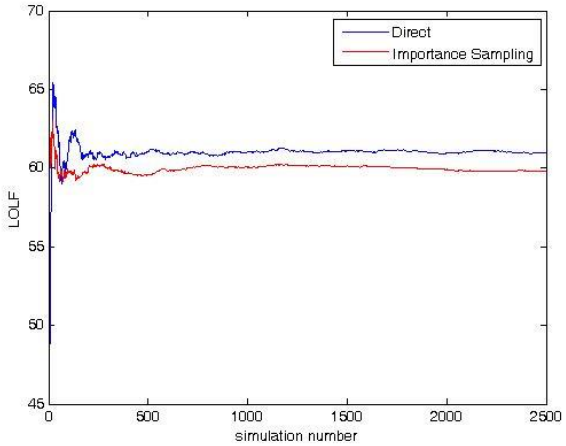

Fig. 3-5 LOLF comparison between the conventional and importance sampling algorithms.

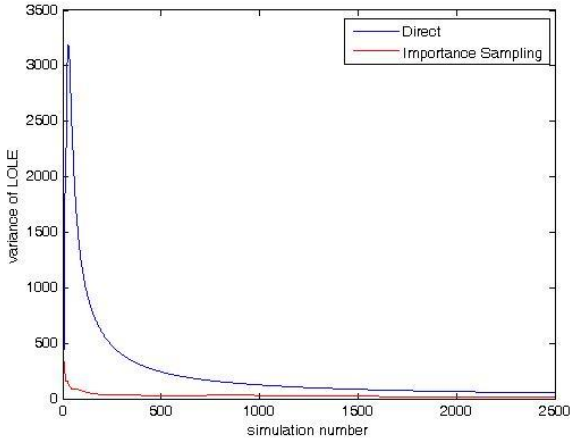

Fig. 3-6 LOLE variance comparison between the conventional and importance sampling algorithms.

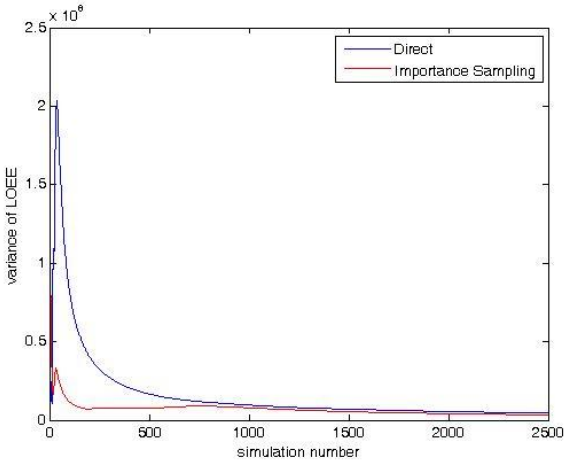

Fig. 3-7 LOEE variance comparison between the conventional and importance sampling algorithms.

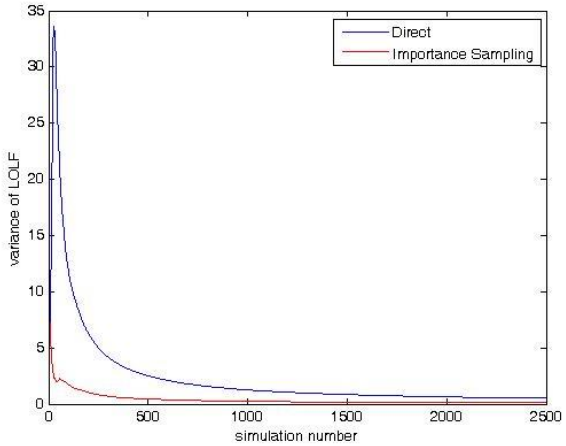

Fig. 3-8 LOLF variance comparison between the conventional and importance sampling algorithms.

From Figs. 3-3 – 3-5, it is observed that there are obvious biases between the two algorithms for two reasons. As explained above, the first is that of the effect of the initial state assumption error. The second is called rounding error. Because the random variables generated in each trial usually are not integers, the random variable is rounded to the closest integer to identify the location in the hourly point axis for each year. That is how rounding error is generated.

3.4 Stratified Sampling

3.4.1 Introduction

For stratified sampling, the region D is broken into m disjoint subregions, D_i, $i = 1,2,\cdots,m$, that is, $D = \cup_{i=1}^{m} D_i$, $D_k \cap D_j = \emptyset, k \neq j$. Defining

$$I_i = \int_{D_i} g(x) f_X(x)\, dx \tag{3-13}$$

and $P_i = \int_{D_i} f_X(x)\, dx$ so that $\sum_{i=1}^{m} P_i = 1$ and

$$I = \int_D g(x) f_X(x) dx = \sum_{i=1}^{m} \int_{D_i} g(x) f_X(x)\, dx = \sum_{i=1}^{m} I_i \tag{3-14}$$

with

$$g_i(x) = \begin{cases} g(x), & if\ x \in D_i \\ 0, & otherwise \end{cases} \tag{3-15}$$

Eq. (3-13) can be rewritten as

$$I_i = \int_{D_i} P_i g(x) \frac{f_X(x)}{P_i} dx = P_i \int_D g_i(x) \frac{f_X(x)}{P_i} dx = P_i E[g_i(X)] \quad (3\text{-}16)$$

where $\int_{D_i} \frac{f_X(x)}{P_i} dx = 1$.

So the estimator is represented as

$$\hat{I} = \sum_{i=1}^{m} \frac{P_i}{N_i} \sum_{k_i=1}^{N_i} g(X_{k_i}) \quad (3\text{-}17)$$

where $\sum_{i=1}^{m} N_i = N$.

Denoting $\sigma_i^2 = Var(g(X_i))$, the variance of this estimator is then

$$Var(\hat{I}) = \sum_{i=1}^{m} \frac{P_i^2}{N_i} Var(g(X_i)) = \sum_{i=1}^{m} \frac{P_i^2 \sigma_i^2}{N_i} \quad (3\text{-}18)$$

Different stratified sampling methods have been proposed in the literature. They are briefly presented next.

I. Optimal Stratified Sampling

It can be proven that $\min\left(Var(\hat{I})\right) = \frac{1}{N}[\sum_{i=1}^{m} P_i \sigma_i]^2$, when $N_i = N \frac{P_i \sigma_i}{\sum_{j=1}^{m} P_j \sigma_j}$ [5].

This method is feasible only if P_i and σ_i can be obtained easily. However, that does not happen usually so there are two other methods based on additional assumptions that may be used.

II. Proportional Stratified Sampling

Since usually one cannot get an exact value for σ_i, It is assumed that $N_i = P_i N$ where P_i can be calculated analytically. It can also be proven that the variance of proportional stratified sampling is not larger than that of Sample-Mean Monte Carlo. Because sometimes it is not known how to choose the proper probability, P_i, one may resort in these cases to the equal stratified sampling as described next.

III. Equal Stratified Sampling

This is also called the systematic sampling method.

Assume

$P_i = \frac{1}{m}$, and $N_i = \frac{N}{m}$, where m is arbitrarily chosen, then

$$\hat{I} = \frac{1}{N} \sum_{i=1}^{m} \sum_{k_i=1}^{N/m} [g(X_{k_i})] \quad (3\text{-}19)$$

In sum, the stratified sampling algorithm divides the sample space into strata and then estimates the target in each stratum. The effective reduction of the variance of the estimation target depends on how much information is known about each stratum, namely, P_i and σ_i.

3.4.2 Stratified Sampling in Power System Reliability

As indicated in the last sub-section, there are three techniques of stratified sampling. Which one is chosen to solve a particular problem depends on the information known about the system under study. In the IEEE RTS case, it is a good idea to group each type of generating unit as one stratum so that there are 9 strata. It is impossible to calculate the P_i and σ_i for the ith stratum ($i = 1,2,\cdots 9$), but it is possible to find another way to get one of them approximately as shown below.

P_i is approximated by the contribution of the ith type of generator to the system capacity, P_i', which is given by

$$P_i' = C_i m_i \frac{MTTF_i}{MTTF_i + MTTR_i} \tag{3-20}$$

where C_i - single generator capacity of the ith type of generator;
m_i – number of generators of the ith type of generator;
$MTTF_i$ – mean-time-to-failure of the ith type of generator;
$MTTR_i$ – mean-time-to-repair of the ith type of generator.

Then P_i' is normalized to get the final $P_i = P_i' / \sum_{i=1}^{9} P_i'$. So the proportional stratified sampling can be approximated by assuming $N_i = P_i N$. Note that the total number of trials for each type of generator should be the same. To this end, the trials are arranged as depicted in Fig. 3-9.

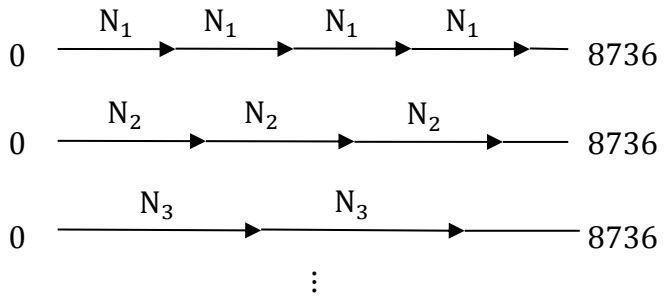

Fig. 3-9 Different types of trial arrangements in stratified sampling.

3.4.3 Case Study

The method discussed above has been applied to the IEEE one-area RTS as well. The same data pre-processing is necessary due to the initial state assumption error. The simulations are repeated for 2500 simulation years for 8736 points each.

The estimators of the three reliability indices, LOLE, LOEE and LOLF, are shown in Figs. 3-10 – 3-12. Compared to the index variances of the conventional Monte Carlo method, the variance reductions of the three indices obtained by the stratified sampling algorithm are significant during the first 100 simulation years. However, as the number of simulation years increases to 2500, two index variances of the stratified sampling estimator are slightly smaller than those of the conventional Monte Carlo method while the third one is not (Figs. 3-13 – 3-15). The reason for that is not clear.

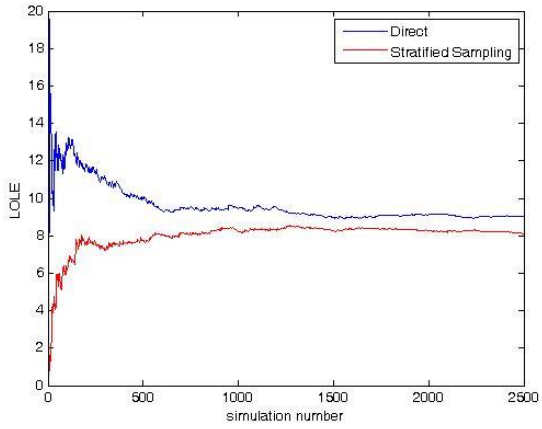

Fig. 3-10 LOLE vs. the number of trials for the conventional and stratified sampling algorithms.

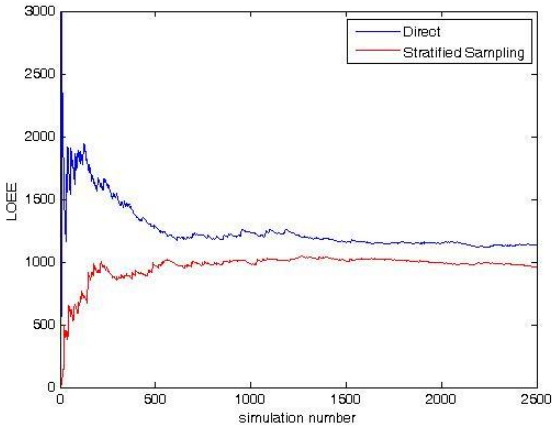

Fig. 3-11 LOEE vs. the number of trials for the conventional and stratified sampling algorithms.

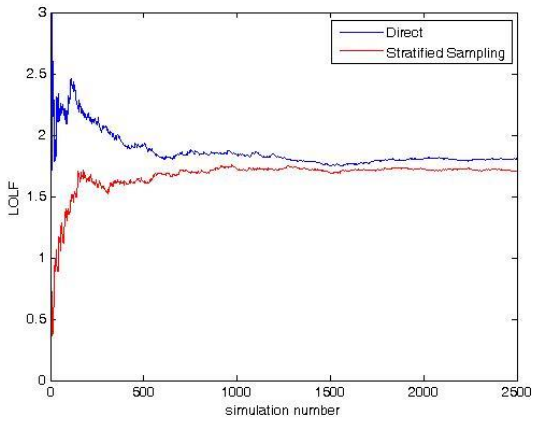

Fig. 3-12 LOLF vs. the number of trials for the and stratified sampling algorithms.

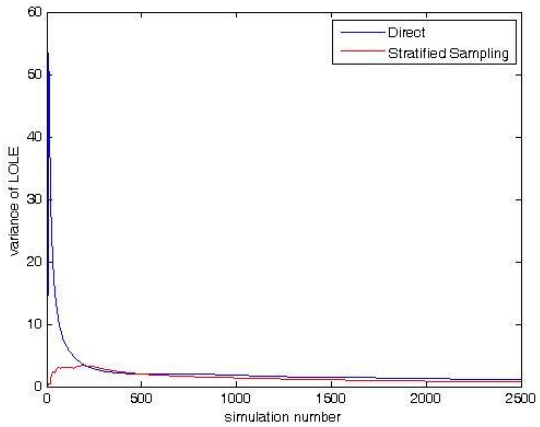

(a)

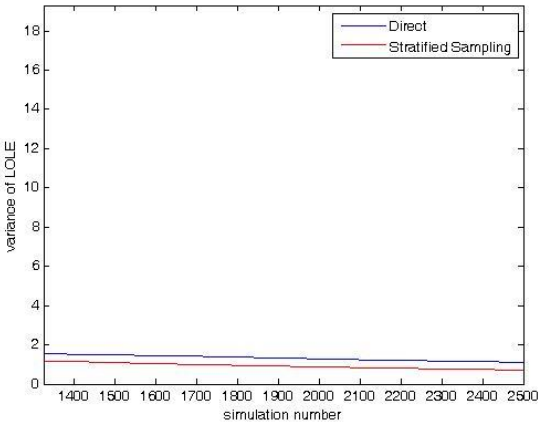

(b)

Fig. 3-13 LOLE variance vs. the number of trials ranging (a) from 1 to 2500 for the conventional and stratified sampling algorithms and (b) from 1300 to 2500 for the conventional and stratified sampling algorithms.

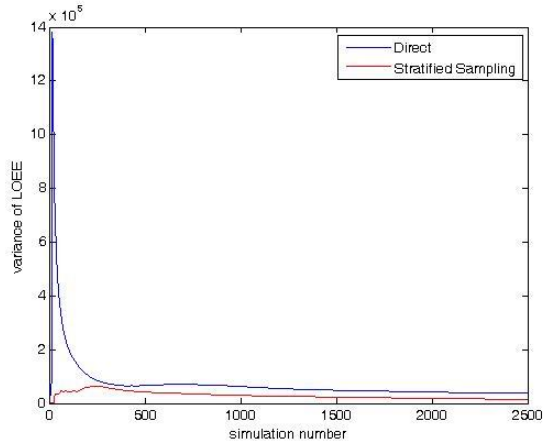

(a)

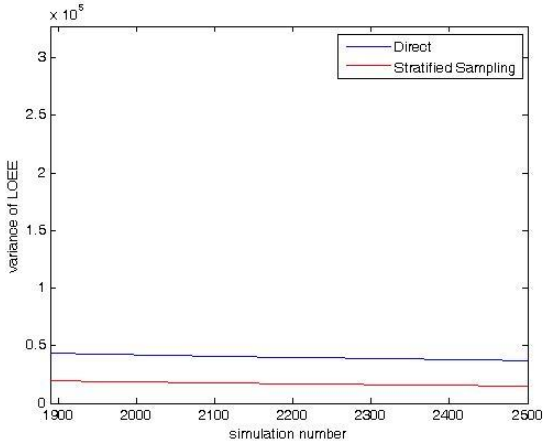

(b)

Fig. 3-14 LOEE variance vs. the number of trials ranging (a) from 1 to 2500 for the conventional and stratified sampling algorithms and (b) from 1900 to 2500 for the conventional and stratified sampling algorithms

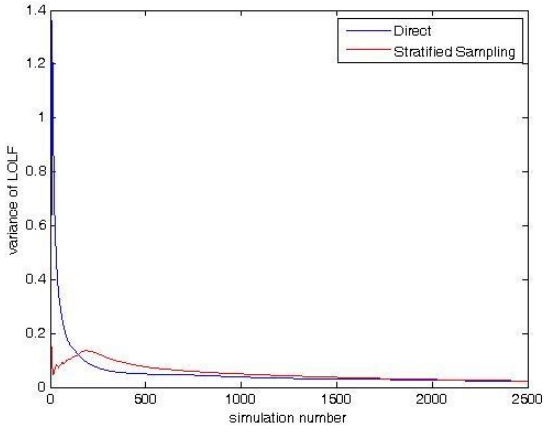

(a)

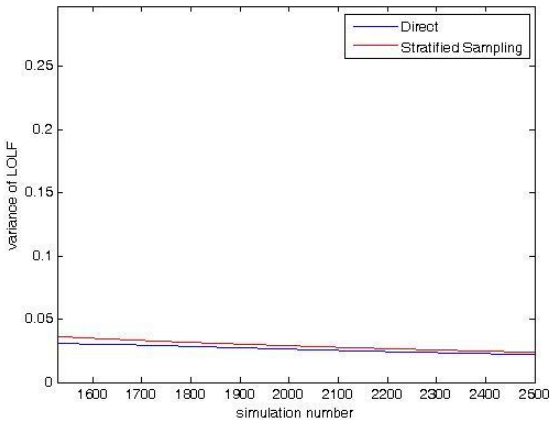

(b)

Fig. 3-15 LOLF variance vs. the number of trials ranging (a) from 1 to 2500 for the conventional and stratified sampling algorithms and (b) from 1500 to 2500 for the conventional and stratified sampling algorithms

3.5 Antithetic Variates

3.5.1 Introduction

The simplest form of the antithetic variates applies only to the estimation of the integral

$$I = \int_0^1 g(x)dx \tag{3-21}$$

This integral can be rewritten as

$$I = \frac{1}{2}\int_0^1 [g(x) + g(1-x)]dx \tag{3-22}$$

The estimator can be represented as

$$\hat{I} = \frac{1}{2N}\sum_{i=1}^{N}[g(U_i) + g(1-U_i)]\,, \tag{3-23}$$

where U_i is a uniformly-distributed random variable.

It can be shown that the variance of the estimator in (3-23) is smaller than or equal to half of the variance of the Sample-Mean Monte Carlo. If the integral given by (3-23) is put into a more general form, the result is

$$I = \int_{-\infty}^{\infty} g(x)f_X(x)dx, \quad x \in R^1. \tag{3-24}$$

Eq. (3-23) then takes into the following form:

$$\hat{I} = \frac{1}{2N}\sum_{i=1}^{N}[g(X_i) + g(X_i')] \tag{3-25}$$

where

$$X_i = F^{-1}(U_i) \tag{3-26}$$

$$X_i' = F^{-1}(1 - U_i) \tag{3-27}$$

and $F(X)$ is the cumulative distribution function (c.d.f.) of X.

In a further step, assume that the domain of $f_X(x)$ is broken up by x_α into two parts with $F(x_\alpha) = \alpha$. Then Eq. (3-25) has the following form:

$$\hat{I} = \frac{1}{N}\sum_{i=1}^{N}[\alpha g(X_i) + (1 - \alpha)g(X_i')] \tag{3-28}$$

where

$$X_i = F^{-1}(\alpha U_i) \tag{3-29}$$

$$X_i' = F^{-1}(\alpha + (1 - \alpha)U_i) \tag{3-30}$$

In the particular case where $\alpha = \frac{1}{2}$, Eq. (3-28) reduces to (3-25).

All associated proofs can be found in [5]. In sum, the antithetic variates method takes advantage of the negative correlation between $g(X_i)$ and $g(X_i')$, where X_i and X_i' are two complementary random variables.

3.5.2 Antithetic Variates in Adequacy Assessment

As indicated in the last sub-section, the application of the antithetic variates technique is straightforward and requires the use of neither an auxiliary function nor known information. One random variable can generate two trials. However, the computational efficiency of the antithetic variates in this problem is not obvious. Actually, most of the computational time is spent on the process after generating random variables. Therefore, the total computational time spent by the antithetic variates method is almost the same as the time spent by the conventional method, although the former method is able to save half of the random variate generating time, which is very little compared to the total computing time. If the same number of random variables is generated, the computation time doubles. In order to keep the same computation time, half the number of random variables is generated in the following case.

3.5.3 Case Study

The method discussed above has been applied to the IEEE one-area RTS as well. The same data pre-processing is necessary due to the initial state assumption error. The simulations are repeated for 2500 simulation years for 8736 points each. Figs. 3-16 – 3-18 show that the estimators of the three reliability indices, namely LOLE, LOEE and LOLF, tend to converge to some value as the simulation proceeds. It is also found that the variance reductions of the antithetic variates algorithm compared with the conventional Monte Carlo method are only mild as the number of simulation years increases to 2500 (Figs. 3-19 -3-21).

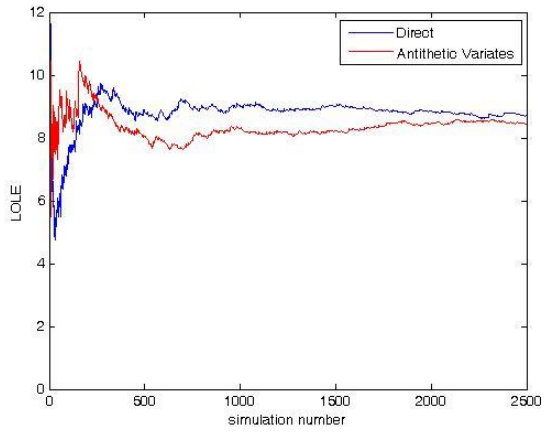

Fig. 3-16 LOLE vs. the number of trials for the conventional and antithetic variates algorithms

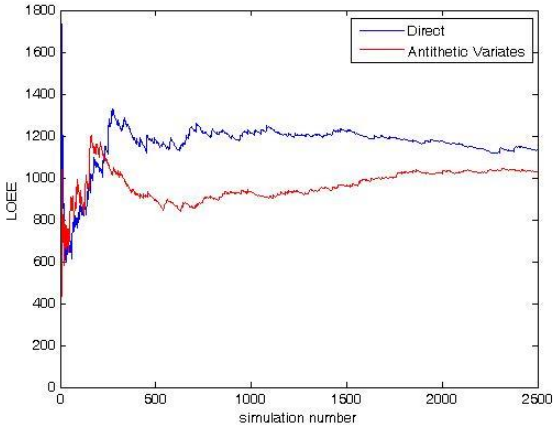

Fig. 3-17 LOEE vs. the number of trials for the conventional and antithetic variates algorithms

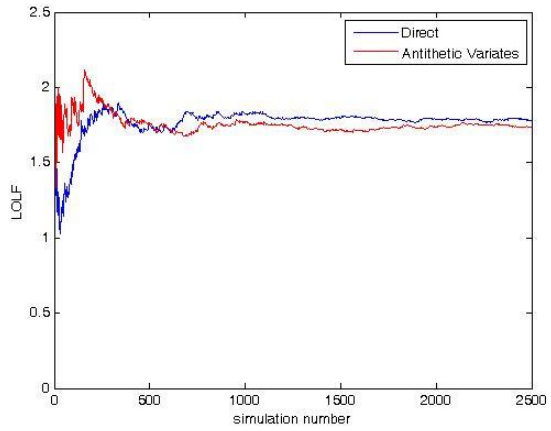

Fig. 3-18 LOLF vs. the number of trials for the conventional and antithetic variates algorithms

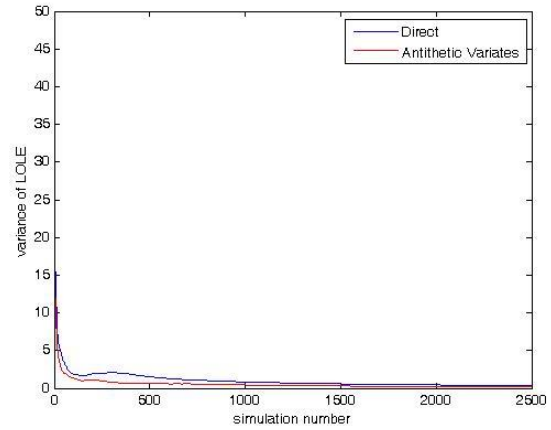

(a)

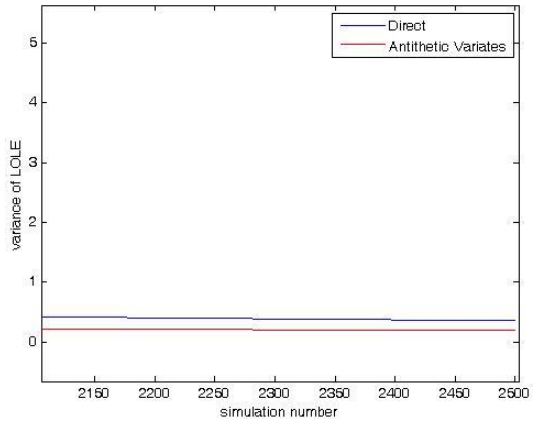

(b)

Fig. 3-19 LOLE variance vs. the number of trials ranging (a) from 1 to 2500 for the conventional and antithetic variates algorithms and (b) from 2000 to 2500 for the conventional and antithetic variates algorithms

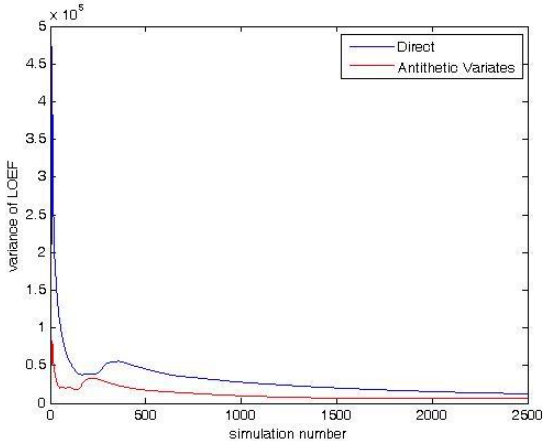

(a)

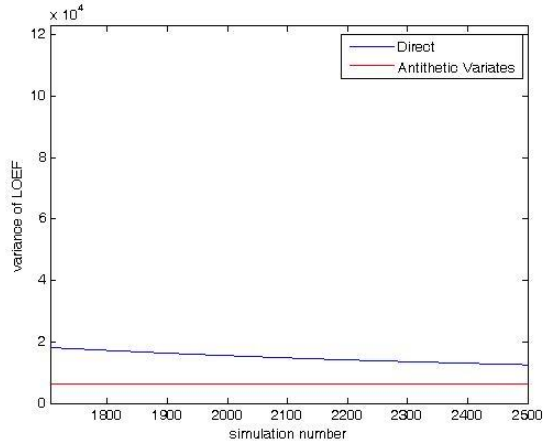

(b)

Fig. 3-20 LOEE variance vs. the number of trials ranging (a) from 1 to 2500 for the conventional and antithetic variates algorithms and (b) from 1700 to 2500 for the conventional and antithetic variates algorithms

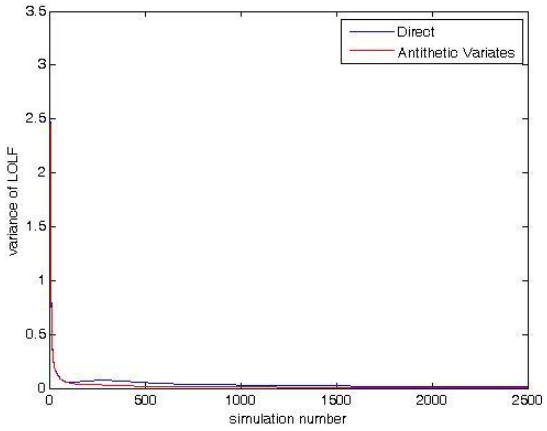

(a)

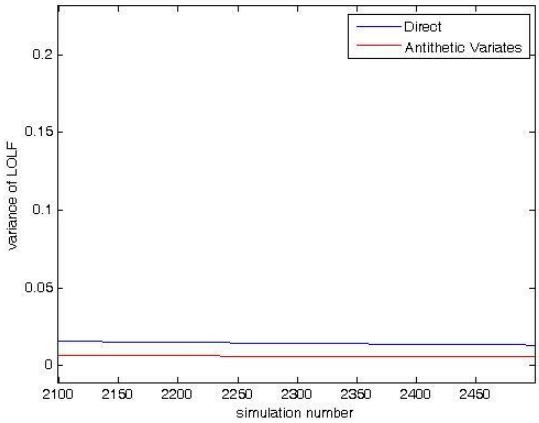

(b)

Fig. 3-21 LOLF variance vs. the number of trials ranging (a) from 1 to 2500 for the conventional and antithetic variates algorithms and (b) from 2100 to 2500 for the conventional and antithetic variates algorithms

3.6 Conclusions

From the power system reliability case study above, the following conclusions regarding the performance of the antithetic variates, the stratified sampling, and the importance sampling methods as compared to that of the conventional Monte Carlo method may be inferred: (i) The variance reduction obtained via the antithetic variates method is small; (ii) The variance reductions obtained via the stratified sampling are not consistent throughout the simulations; (iii) In contrast, the variance decrease of the importance sampling algorithm is good. However, more tests are needed to confirm this result since the use of the Rayleigh distribution is new to this method.

Chapter 4

Composite Power System Vulnerability Evaluation to Cascading Failures Using Importance Sampling and Antithetic Variates

4.1 Introduction

Power Systems operate under the risk of major disturbances that may induce large-scale blackouts, which are costly to society. One typical example is the 2003 U.S.-Canada blackout, whose total estimated costs incurred by the United States economy range between 4 to 10 billion U.S. dollars. In Canada, the gross domestic product suffered a decrease of 0.7% in August 2003 while the work hour losses amounted to 18.9 million. In Ontario, manufacturing shipments decreased by 2.3 billion Canadian dollars [1]. This blackout has prompted the development of new approaches and methodologies aimed at assessing and managing the risk of cascading failures in power systems.

The need to secure a continuous supply of electric energy for a modern nation has raised major concerns about power system reliability. These concerns have promoted system reliability analysis as one major research endeavor in power systems. Seminal work in this area has been carried out by Billinton *et al.* [21], [6], [45]. However, the methods and algorithms proposed by the authors do not model cascading failures. The latter include cascading overloads, failures of protection devices, transient instability, forced or unforced initiating failures, shortage of reactive power, voltage instabilities and voltage collapse, computer failures at the control center, unavailability of Energy Management System (EMS) functions for security monitoring and analysis such as power system state estimation and contingency analysis, lack of situational awareness, communications mistakes, and operational errors. In general, large-scale blackouts stem from the occurrence of a combination of several of these failures. While several papers in the literature (*i.e.*, [14], [45], [8]) have investigated each of these failures independently from each other, they have not provided a general framework for analyzing them as a combined phenomenon.

By contrast, Wang *et al.* [28] develop a canonical steady-state Markov model that is implemented via DC power flow to simulate cascading outages, whose transition

probabilities are estimated while taking into account the uncertainty of the generation and line overloads modeled as Gaussian random variables. Anghel *et al.* [27] propose a stochastic model that includes human factors and line sagging while modeling the maximum power flow of a line as a function of its power rating and the temperature of the environment. Hardiman *et al.* [25], [43] and Kirschen *et al.* [26] make use of a transient Markov chain to model cascading outages, which may lead to system blackouts. In [26], the restoration time is assumed to depend on the amount of load to be reconnected.

As indicated in [45], protective relays play an important role in 73.5% of major disturbances. Consequently, the protection system should be taken into account when analyzing the risk of cascading failures. In composite power systems, the major protective devices involve over-and under-voltage relays on generator, under-voltage relays on large-capacity motors, and impedance and over-current relays on transmission lines. Thorp *et al.* [14], [46], [42] apply an empirical hidden failure probabilistic model to the zone 3 relays of all the lines incident to a given line, while Mili *et al.* [7], [8] apply short-circuit analyses to identify all the relays exposed to hidden failures. The former model has not been proved while the later method is cumbersome. Singh *et al.* [30], [31], [32] have extended various power system reliability models to account for failure rates of protection systems, including hidden failures. In [30], the authors establish a seven-state protection component model, while in [32], they derive a four-state simplified component model from the complete Markov model for protection system failures. Unfortunately, the unavailability of a large historical data set precludes them from estimating with sufficient accuracy the transition rates of the complete Markov model.

According to the 2003 U.S.-Canada blackout [1], tree contact is one of the critical factors that push the system operating point toward the edge of collapse. The combination of heavy-loaded transmission lines and overgrown trees may increase the risk of tree contact failure. Although some researchers have developed models of sag-tension of overhead transmission lines through conductor thermal strains and physical characteristics, ambient temperature, creep time and so on [9], [10], [11], there is still a need of a simple but realistic model of this phenomenon for cascading failure simulations.

Since an exhaustive computation of detailed modeling for all possible combinations of failures is infeasible, simplification and approximation are needed in modeling and analyzing cascading failures. For example, there is an extensive literature on cascading failure that takes a high level approach and neglects the power loading of a power system [12], [13]. However, power flow pattern changes after each outage have an effect on the likelihood of subsequent outages. Some attempt to reduce the sampling size by applying an importance sampling technique has been made by Thorp *et al.* [14], [42] based on the

assumption that the failure probability follows the Bernoulli distribution. Singh *et al.* [33], [34], [35] reduce the computation effort by using state space pruning and partitioning methods, which can be implemented in non-sequential Monte Carlo simulations. The latter procedure has been utilized by Kirschen *et al.* [26] in conjunction with a stratified sampling technique to divide the total system load into a number of presumed strata so that the number of trails is reduced.

Billinton *et al.* [21], [6] have made some progress by applying two types of variance reduction techniques, namely, control variates and antithetic variates in power system reliability evaluation to decrease the computing time burden of the simulations. The speedup provided by these techniques can reach a factor of 3.33 or more for the 6-bus Roy Billinton Test System (RBTS). But their efficiencies are very much model dependent [6]. Only antithetic variates techniques have been applied to a larger system, namely, the 24-bus IEEE Reliability Test System (RTS) [18], with a speedup factor of 2. This has prompted a further investigation here of these techniques when simulating cascading failures.

An interesting probabilistic indicator is proposed by Kirschen at al. [26] to quantify the vulnerability of a power system to various cascading failure scenarios. Specifically, they advocate the use of the Expected Energy Not Supplied (EENS) as an indicator of system stress because it incorporates in a straightforward manner all the relevant reliability indices, including the Loss of Load Probability (LOLP) and the Loss of Load Expectation (LOLE). In the work here, this indicator is incorporated into a general composite Monte Carlo reliability analysis of cascading failure in power systems.

This chapter describes a risk-based method for composite power system vulnerability evaluation to cascading failures via sequential Monte Carlo simulations. Numerous scenarios with a feasible sampling size are considered so that the risk of cascading failure is reasonably estimated when achieving power system expansion. To decrease the computational burden, an importance sampling technique utilizing the Weibull distribution is applied to the generator outages. For further improvement, another method is proposed which combines importance sampling and antithetic variates together. This combined method is only applied the generator outages, because the antithetic variates algorithm is not suited to the simulation of transmission line outages in the state sampling approach. It is shown that the importance sampling algorithm requires roughly one-third to one-half of the number of samples required by the conventional Monte Carlo method to reach a desired level of accuracy depending on the system under test, while the combined method decreases this ratio even further. To illustrate and evaluate the developed approach, two case studies are conducted and analyzed on the IEEE one area RTS and the IEEE three area RTS [18], respectively.

This Chapter is organized as follows. Section 4.2 deals with sequential Mote Carlo modeling considering cascading failures. Section 4.3 is devoted to the implementation of the importance sampling method, while Section 4.4 proposes the importance sampling and antithetic variates combined method. Section 4.5 then discusses the other variance reduction techniques. Section 4.6 describes two case studies on the IEEE one-area and three-area RTS.

4.2 Sequential Monte Carlo Modeling Considering Cascading Failures

When modeling cascading failures in composite reliability analysis, sequential Monte Carlo simulations require the implementation of prohibitively large sampling sizes. This is mainly due to the need to model many types of failures and many different mechanisms by which failures propagate if all possible real system scenarios are taken into account. The simulations also involve a variety of modeling requirements at multiple timescales since electromechanical phenomena occur in seconds while voltage support devices and thermal heating effects occur in minutes. It is therefore necessary to find a trade-off between simulation accuracy and computational burden. The way to achieve this tradeoff is explained next.

4.2.1 Sequential Monte Carlo Simulations

Since system failures may cascade in numerous ways, Monte Carlo simulations are the methods of choice. These techniques estimate system responses by implementing and executing a series of plausible scenarios. Generally speaking, there are three different simulation approaches in reliability evaluation [45]. Firstly, in the state sampling approach, a uniformly distributed random variable is generated to decide whether the component state is in failure or not. That is, if the random variable is larger than the failure probability, the component is in the normal state; otherwise, it fails. The system state is the combination of all component states. Secondly, the state duration sampling approach uses the component state duration distribution functions. In a two-state component representation, these are operating and repair state duration distribution functions, which are usually assumed to be exponentially distributed. Finally, in the state transition sampling approach, there is a transition probability that represents the probability of the departure from the previous state to the present state in the time domain. Most of the related applications are based on a steady-state Markov chain where the transition rates are usually assumed to be constant, which is not realistic in a typical process of cascading failures as argued in Section 4.1.

The state sampling method is not considered here because of its inability to model the restoration procedures of the system components, while the state transition sampling approach fails to vary the transition probabilities when a sequence of dependent events propagate successively over a time span. The latter characteristic stems from the changing likelihood of subsequent outages that hinge on system power flow patterns. It turns out that the state duration sampling approach does not have these weaknesses. Combined with annual chronological load curves, it provides a relatively realistic framework for simulating cascading events. It is this method that has been implemented and tested. It will be described next.

4.2.2 Basic Reliability Model

Sequences of dependent cascading failures involve the actions of various components and devices, which include over- and under-voltage relays on generators and large-capacity motors, zone 3 impedance relays on transmission lines, and vegetation under transmission lines. Now, the actions of these components hinge on system power flow and nodal voltage patterns. Consequently, their simulations require the execution of full AC power flow calculations over a certain time interval, which is set to one hour or more, as the vulnerability evaluation aims at long-term power system planning. They also involve the execution of constrained optimal power flow calculations, where the generators' capacities instead of their exact output powers are provided. Note that these simulations need the specification of the forced outage rates of the generators and the transmission lines.

4.2.3 Effects of Relays on Cascading Failures

Over- and under-voltage relays protect most generators while under-voltage relays protect large-capacity load motors (equal or larger than 750 MVA) [15] and certain other equipment. While in general these relays operate as intended, their operations will reduce the angular and voltage stability margins of the system in the course of a sequence of cascading failures.

Impedance protective relays are the major protective devices of high voltage transmission lines. Generally, they operate when the measured impedance falls within the relays' setting range. Unfortunately, as observed during the 2003 US-Canada blackout, they may unduly overtrip during cascading failures due, for example, to voltage sags and line overloads. The latter make the measured impedance by a relay smaller than its setting, simulating a nearby fault on the system. Note that among impedance relays, zone 3 relays are the most sensitive to voltage dip due to their large setting range [1].

4.2.4 Simplified Model of Vegetation effects

The occurrences of tree-contact faults are usually taken into account by forced outage rates in reliability evaluation, which are estimated from historical data. Is this approach correct? Obviously not since sequences of tree-contact faults typically occur due to load transfer in the transmission network following line outages. A typical mechanism is as follows. Heavily-loaded transmission lines have typically high conductor temperatures due to the thermal characteristic of the conductors, particularly when the ambient temperature is high. This results in large line sags, which in turn increases the probability of tree contacts. This is one reason why more cascading failures occur during the summer time than during colder seasons.

The detailed model of overhead conductor sag is complex, which includes modeling of conductor metal thermal strain, elastic strain, settling strain, and creep strain, conductor arc length, half-span and weight, line current, ambient temperature, wind speed, wind direction, and so on. To improve the efficiency of these calculations, a simplified model is proposed that is effective and efficient in cascading failure simulations. A crude relationship between conductor temperature and current is proposed in [16]. It is based on the assumption that the conductor temperature change is proportional to the amount of heat produced by the conductor, which is proportional to the square of the current in the conductor as follows:

$$\theta_F = \theta_0 + (\theta_e - \theta_0)\left(\frac{I_F}{I_e'}\right)^2. \tag{4-1}$$

Here θ_0 is the ambient temperature around the conductor; θ_e denotes the maximum temperature limit of the conductor in normal operation; I_F is the maximum long-term current in the conductor; and I_e' is the maximum limit of the current in the conductor, which is a modified value of the rated current of the conductor. It is given by

$$I_e' = I_e\sqrt{\frac{\theta_e-\theta_0}{\theta_e-\theta_{0e}}}. \tag{4-2}$$

where I_e denotes the rated current of the conductor, θ_{0e} is the ambient temperature around the conductor set together with the rated current I_e and the temperature limit θ_e.

The graph relating the measured sag and the conductor temperature shown in Figs. 5 and 6 in [9] and Fig. 6 in [10], respectively, exhibits an approximate linear relationship when the conductor temperature is within its normal working range. It is therefore reasonable to assume in our simulations that the sag is proportional to the conductor temperature as follow:

$$sag = (\theta_F - \theta_e)a. \quad (4\text{-}3)$$

Here a is set at $0.01\,m/℃$ based on Figs. 5 and 6 in [9] and Fig. 6 in [10]. Another assumption made is that the height of the vegetation under the transmission lines is assumed to be a normal random variable.

In the simulation, for each transmission line, I_e' is updated after each time interval, while a power flow or optimal power flow calculation gives the current value of I_F at that time point. The current conductor temperature θ_F is then calculated by (4-1) and the conductor sag is given by (4-3). Based on the assumed normal distribution of the vegetation height, the distance between the bottom of the sag and the top of the tree is normally distributed with a certain cumulative probability distribution function (c.d.f.), as the heights of the transmission towers are constant. The probability of tree contact is computed by the above CDF.

4.2.5 Modeling Power System Restoration

One critical step in the approach here is to model power system restoration. However, restoration models may become rather complex if they represent all the multiple stages involved in any restoration, the combination of which depends on system properties. As discussed in [36], the restoration of power systems with non-blackstart generators generally includes the following sequence of events: (1) start up the blackstart units to provide cranking power for non-blackstart units; (2) energize separate load islands; and finally (3) synchronize these islands. It is worth noticing that some utilities implement other procedures specific to them. For example, Hydro-Quebec prefers to recover the transmission grid before the cranking of non-blackstart units [36]. Because power system restoration may take different paths, while including numerous operational constraints, researchers have relied on some heuristic methods such as multi-agent techniques [39] and fuzzy rules [38] rather than applying more formal modeling methods.

Our approach for modeling system restoration has been inspired by the work of Hou *et al.* [36] and Ozog *et al.* [37], who independently have shown that the energy not supplied exhibits a linear growth with ups and downs as the restoration time increases. This prompted modeling the energy not supplied as a straight line segment starting from the origin and ending at the total load demand over a period of 2 hours. The rationale for the choice of that time period is that in the Monte Carlo simulations, the likelihood ratio tests indicate with a good degree of confidence that the power law distributions better describes the variability of the energy not served per failure as demonstrated in Section 4.6.2. This is in agreement with results obtained when using actual outage data for the US power system [40], [41].

4.2.6 Algorithm of the Developed Monte Carlo Procedure

The developed Monte Carlo simulation procedure depicted in Fig. 4-1 is briefly summarized as follows:

(1) Set all the relays as normally closed and the tree contact probabilities equal to zero;
(2) Draw random samples for time-to-failure or time-to-repair of the generators if their previous states end;
(3) Check the under- or over- voltage relay states on the buses;
(4) Draw random samples and determine if the lines are tripped due to the forced outage rate and the tree contact probability;
(5) Check the zone 3 impedance relay states on the lines;
(6) Adjust initial data and run an AC power flow program, then go to (7) if it converges; otherwise go to (9). Here, AC power flow calculations are executed separately if the network is separated, where the generator bus with the largest generation capacity in the new sub-system is selected as the slack bus;
(7) Check if there is any voltage or reactive power violation, then go to (8) if yes; otherwise go to (11);
(8) Do PV-PQ switching for those buses whose reactive power constraints have been violated; otherwise, cut off some loads on the violated buses, then go to (10);
(9) Shed some loads by DC optimal power flow calculation, then go to (10) if this calculation is successful, otherwise go to (14);
(10) Run the AC power flow solution, then go to (11) if it converges; otherwise go to (14);
(11) Calculate the load curtailment in MW as the energy not supplied in this time interval and record it;
(12) Update all relay states and the tree contact probabilities;
If it is the end of a year, calculate the energy not supplied for this year and go to (14), otherwise, go to (2);
(13) If the maximum simulation years have not been reached, go to (2);
(14) Assume this scenario as a voltage collapse, and set the system restoration process to 2 hours; then return to (1).

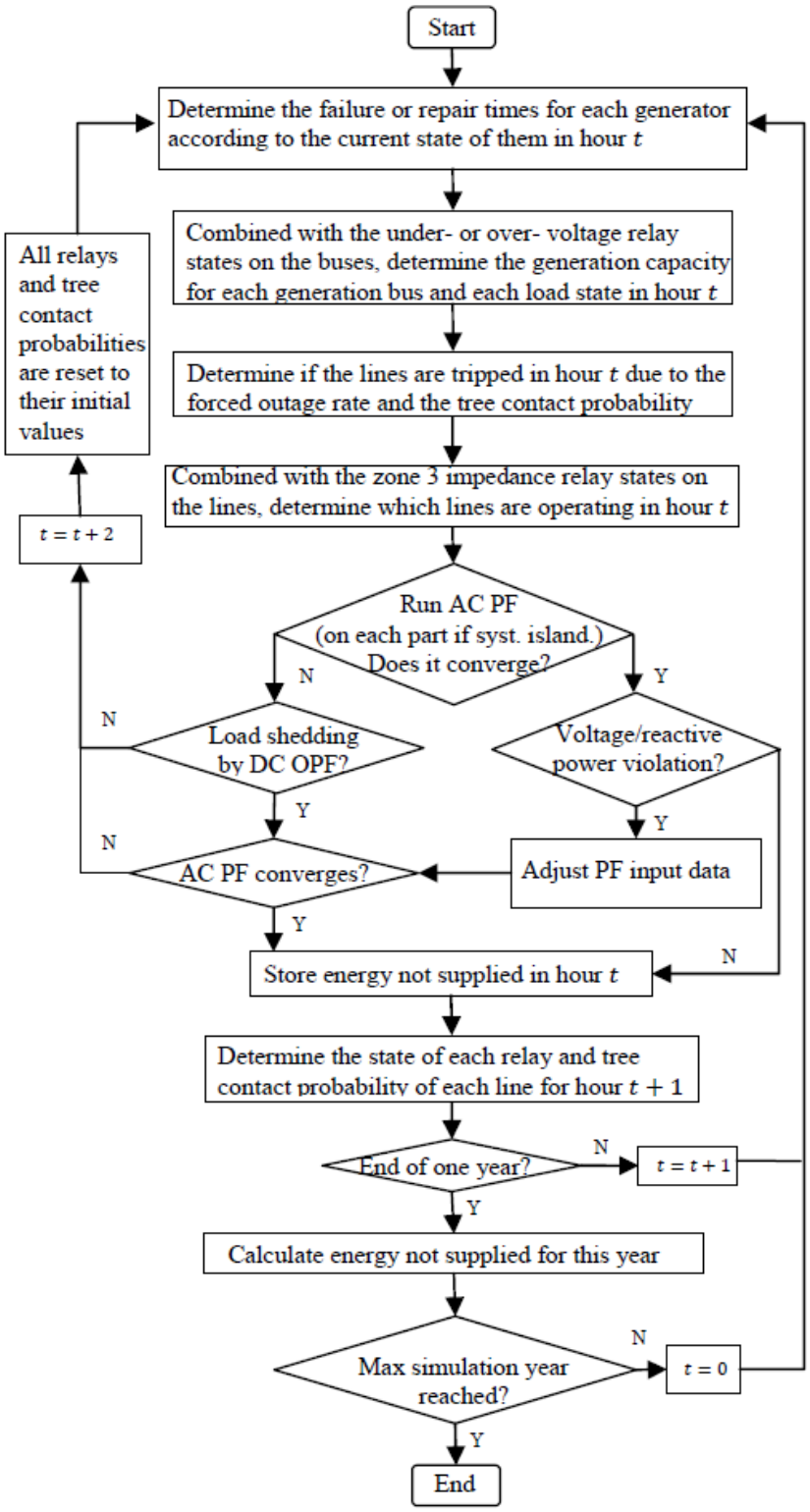

Fig. 4-1 Flowchart of the developed Monte Carlo procedure.

4.3 Importance Sampling Method in Composite Power System

Monte Carlo methods can be used to estimate the mean value of a random variable via a sample-mean estimator with a large number of trials. Variance reduction techniques aim at decreasing the number of Monte Carlo trials while maintaining a desired level of accuracy by reducing the variance of the sample-mean estimator under study based on known information about the problem. There are several well-known variance reduction techniques, including importance sampling, control variates, stratified sampling, antithetic variates, and daggering sampling.

Importance sampling achieves variance reduction of the sample mean of a random sample drawn from a given probability distribution by calculating instead the weighted sample mean of a random sample drawn from another distribution. The weights assigned to the latter samples are chosen so that the weighted sample mean tends to the true mean of the original distribution with a smaller variance.

In power system reliability analysis, the intent is to apply the importance sampling method to estimate the Expected Energy-Not-Served (EENS). But this method requires the a priori knowledge of the probability distribution of the random variable whose mean value has to be estimated. Unfortunately, the energy-not-served follows a distribution that is unknown a priori and varies in different systems. On the other hand, the distribution of the time-to-failure is known since it is usually assumed to be an exponential distribution. Furthermore, its mean value, the so-called Mean-Time-to-Failure (MTTF), is related in a straightforward manner to LOLE and EENS. Therefore, the approach here is to apply importance sampling to estimate MTTF and then to infer an estimate of LOLE and EENS. Note that in the case where a system undergoes a minor change, it is possible to directly apply the method to the energy-not-supplied to gain more variance reduction if the distribution of that variable has been determined beforehand.

In Monte Carlo simulations, the time-to-failure and time-to-repair, T, associated with the chronological state changes of generators are assumed to follow an exponential distribution with a p.d.f. given by

$$f_e(t) = \lambda e^{-\lambda t} , \tag{4-4}$$

where λ is the mean value of this distribution. It follows that the generator mean-time-to-failure (MTTF) is given by

$$MTTF = \int_0^\infty t f_e(t) dt . \tag{4-5}$$

If another random variable X with a p.d.f. $f_X(X)$ is chosen instead of the original exponential distributed random variable, T, then we can write the MTTF can be written as

$$MTTF = \int_0^\infty \frac{x f_e(x)}{f_X(x)} f_X(x) dx \,. \tag{4-6}$$

A least-squares estimator of MTTF is expressed as

$$\widehat{MTTF} = \frac{1}{N} \sum_{i=1}^{N} \omega_i X_i, \tag{4-7}$$

where $\{ \omega_i = \frac{f_e(X_i)}{f_X(X_i)}$, i=1,…, N$\}$ are the weights that will make (4-7) an unbiased estimator of the MTTF when processing samples drawn from the new p.d.f., $f_X(X)$, instead of the original one, $f_e(X_i)$.

Another form of (4-7) can be derived by replacing the time-to-failure, T, by a function $h(X)$ expressed as

$$h(X) = \frac{X f_e(X)}{f_X(X)} \,. \tag{4-8}$$

Substituting (4-8) into (4-7) yields

$$\widehat{MTTF} = \frac{1}{N} \sum_{i=1}^{N} h(X_i). \tag{4-9}$$

Note that here the samples are those of the random variable, X, not of T.

Obviously, a variance reduction is obtained if

$$var[h(X)] < var[T]. \tag{4-10}$$

where

$$\begin{aligned} var[h(X)] &= \int \frac{x^2 f_e^2(x)}{f_X(x)} dx - MTTF^2 \\ &\geq (\int x f_e(x))^2 - MTTF^2 = 0. \end{aligned} \tag{4-11}$$

The inequality (4-11) can be derived using the Cauchy-Schwarz inequality [5], the equality of which is tenable when the random variable X is distributed according to a p.d.f. given by

$$f_X(x) = \frac{x f_e(x)}{MTTF}. \tag{4-12}$$

This means that the largest possible variance reduction is obtained when $f_X(x)$ is given by (4-12) since in that case, $var[h(X)] = 0$, which indicates that $h(X)$ is no longer

random. In practice, $f_X(x)$ is chosen to be close to that expression so that $h(X)$ is still a random variable. Substituting $f_e(x)$ given by (4-4) in (4-12) and setting $MTTF = 1/\lambda$ yields

$$f_X(x) = \lambda^2 x e^{-\lambda x}, \tag{4-13}$$

which is the p.d.f. of a Gamma distribution. If this distribution is used for X in the simulation, synchronous generators of the same type start and shut down at the same time, which is not realistic. To overcome this problem, a p.d.f. must be chosen that approximates (4-13) as the induced importance sampling p.d.f., $f_X(x)$. In these simulations, the Weibull PDF is used and is expressed as

$$f_w(x) = \frac{\beta}{\alpha}\left(\frac{x}{\alpha}\right)^{\beta-1} e^{-\left(\frac{x}{\alpha}\right)^{\beta}}. \tag{4-14}$$

The Weibull parameter values may be obtained via an estimation method, for example, via a least-squares method. In the example depicted in Fig. 4-2, the two parameters α and β are respectively estimated as $\alpha = 2105$ and $\beta = 1.55$ while $\lambda = 0.001$. The comparison of $xf_e(x)$ to the scaled Weibull p.d.f. is depicted in Fig. 4-2.

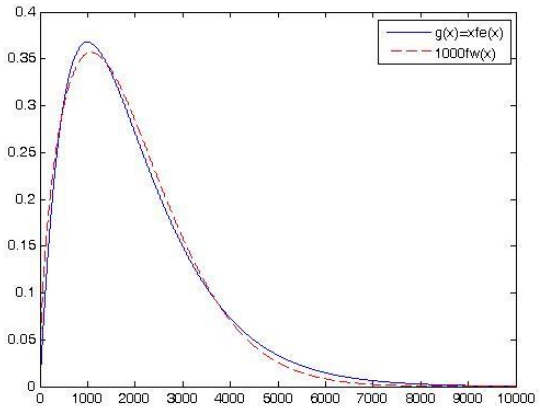

Fig. 4-2 Comparison of $xf_e(x)$ and the scaled p.d.f. of the Weibull distribution.

Applying the importance sampling method, Eq. (4-6) is replaced by

$$MTTF = \int_0^{\infty} \frac{xf_e(x)}{f_w(x)} f_w(x)dx\,. \tag{4-15}$$

An unbiased estimator is given by

$$\widehat{MTTF} = \frac{1}{N}\sum_{i=1}^{N} h(X_i)\,, \tag{4-16}$$

where $h(X) = \frac{X f_e(X)}{f_w(X)}$. Here the random variates X_i are drawn from the Weibull distribution. By choosing a set of appropriate parameters, α and β, so that $f_w(x)$ is close to the exact p.d.f., $f_X(x)$, given by (4-13), the variance of $h(X)$ can be made smaller than that of the time-to-failure, T. This leads to a greater simulation precision under the same number of samples. Note that the same procedure is applied to estimate the mean-time-to-repair, μ.

4.4 Importance Sampling and Antithetic Variates Combined Method

Another well-known variance reduction method is the antithetic variates method, which is able to induce a variance reduction by means of a negative correlation between two simulation trials in any pair of two complementary random variables. As an example, consider a mapping, $Y = g(X)$, which is induced by a uniformly distributed random variable $X \sim U[0,1]$. The sample X_i and $1 - X_i$, which are perfectly negatively correlated, generate a pair of $g(X_i)$ and $g(1 - X_i)$. If $g(x)$ is a continuous, monotonically, non-increasing (or non-decreasing) function with continuous first derivatives, the variance of the sample-mean estimator given by

$$\hat{Y} = \frac{1}{N}\sum_{i=1}^{N/2}[g(X_i) + g(1 - X_i)] \tag{4-17}$$

is significantly reduced. Here N is an even integer larger than 2.

The application of the above antithetic variates method to a uniform distribution can be expanded to any other distributions with closed form expressions. Denote the c.d.f. of a given random variable Z by $F(z)$. A pair of strongly negatively correlated samples Z_i and Z_i' can be generated from a pair of seeds, X_i and $1 - X_i$, via the inverse method as follows:

$$Z_i = F^{-1}(X_i) \tag{4-18}$$

$$Z_i' = F^{-1}(1 - X_i)\ . \tag{4-19}$$

The antithetic variates algorithm has been successfully applied to power system reliability evaluation by Billinton *et al.* [4, 6], who obtained a good decrease in computational burden, even though the estimated reliability indices cannot be expressed as continuous monotonic functions with continuous first derivatives, which is the sufficient condition for its application as proven in [5]. Their work is extended here later.

Recently, Thorp *et al.* [14] applied importance sampling to assess the risk of power system blackouts by modeling hidden failures of transmission line zone-3 relays. However, their method is not suited to composite reliability analysis because it cannot

account for power generator random outages involved in the state duration sampling. By contrast, the variance reduction approach developed here can do that analysis by applying importance sampling and antithetic methods in a separate way to power generator and transmission line outages.

The application of antithetic variates to power generators is discussed first. Although a reliability index such as the expected energy not supplied (EENS) cannot be expressed as a continuous function for a time-to-failure or time-to-repair of a power generator, the EENS has a non-increasing relationship with the availability of the power generator, while everything else remains the same. Because the availability of a power generator changes in the same way as the time-to-failure and the opposite way as the time-to-repair, the EENS has a monotonic relationship with time-to-failure and time-to-repair.

As for transmission line outages, the simulations here have shown that the antithetic variates method does not result in a significant variance reduction. One possible explanation is that there is no monotonic relationship between EENS and the uniformly distributed random variable upon which the state of a line is inferred. Therefore, for the transmission lines, neither the importance sampling nor the antithetic variates method is applied.

In further investigation, it is found that it is possible to achieve a larger variance reduction by combining the importance sampling method and the antithetic variates method together in power system reliability evaluation. Based on the importance sampling method, random samples are drawn from the Weibull distribution instead of the exponential distribution. Here random samples are generated by (4-18) and (4-19) with the Weibull c.d.f.. Since the simulation is executed sequentially, Z_i is first used to obtain the time-to-failure or time-to-repair as

$$\xi_i = h(Z_i) = \frac{Z_i f_e(Z_i)}{f_w(Z_i)}, \tag{4-20}$$

while Z_i' is pushed into a stack temporarily. The time-to-failure or time-to-repair is replaced by the ξ_i given by (4-20) in the importance sampling algorithm depicted in Section 4.3. After the trial observation of Z_i has been obtained, Z_i' is popped out and addressed in the same way to get the complementary trail observation. Finally, an estimate, $\hat{Y}$, is calculated via

$$\hat{Y} = \frac{1}{N}\sum_{i=1}^{N/2}[g(\xi_i) + g(\xi_i')] \,. \tag{4-21}$$

In this way, the combined method takes advantage of both the importance sampling and antithetic variates techniques.

4.5 Other Variance Reduction Techniques

As for other variance reduction techniques – correlated variates, stratified sampling and dagger sampling, it is found that they do not lead to a significant variance reduction in power system reliability analysis. The correlated variates method makes use of the correlation between the estimation target and an auxiliary random variable whose expectation is already known. The simulations here show that it performs well on the 6-bus RBTS [21], [6]. However, no attempts have been made on any larger systems. The stratified sampling is based on an idea similar to that of importance sampling. For this method, the sampling region is divided into a number of disjoint subregions and their relative importance is assessed. Those subregions deemed to be the most important will be sampled more than the others, yielding a variance reduction of the estimator of the reliability index of interest. This method has been applied by Marnay *et al.* [22] to assess the adequacy of a power system with no transmission constraints. Regarding dagger sampling, while its methodology is similar to that of antithetic variates, it is only suited to two-state random variables, therefore, can only be applied to transmission line states, not to power generator states. It has not been incorporated into the approach here because it leads to minor variance reduction, the reason being that the states of the transmission lines have no monotonic relationship with the estimation target.

4.6 Two Case Studies Using Two IEEE Reliability Test Systems

The developed methods have been applied to the IEEE one-area RTS and the IEEE three-area RTS, whose data are provided in [17], [18]. The initial condition for the simulations is a normal operating case of the system without any generator or transmission line outages. The average temperature data of the city of Falls Church in Virginia [19] is taken as the ambient temperature data, which contains three temperature intervals per day throughout a whole year. All the random numbers needed in the simulations are generated by the *.NET* Random class, which is based on a modified version of Knuth's subtractive random number generator algorithm [20] where the number of milliseconds elapsed since computer system start is used as the random seed.

Sequential Monte Carlo simulations involving cascading failures have been carried out to evaluate the EENS for long-term power system planning. The outcomes of the Monte Carlo simulation include the sample mean, $\hat{\mu}$, and the sample variance, $\hat{\sigma}^2$, of EENS from a sample of size N, which allows one to calculate the coefficient of variation C_v defined as

$$C_v = \frac{\sqrt{\sigma^2/N}}{\mu}. \qquad (4\text{-}22)$$

The coefficient of variation is used to weigh the simulation precision.

4.6.1 Case I – IEEE one-area RTS

The IEEE one-area RTS that was published in 1996 has 32 generating units with a total installed capacity of 3405 MW and has 24 buses connected by 38 transmission lines. Since only hourly data are available for the load curves, the time unit of the simulations is one hour.

Fig. 4-1 provides the flowchart the our simulations conducted here. In these simulations, it is assumed that a voltage collapse has occurred if the AC power flow diverges owing to an ill-conditioned or a singular Jacobian matrix. In this case, all the loads are arbitrarily curtailed for 2 hours to recover the system.

Three types of random variables are implemented in the simulations, namely, the time-to-failure and time-to-repair of generators along with the transmission line states. The conventional method draws random variates of time-to-failure and time-to-repair from the exponential distribution, while the importance sampling (IS) method uses the Weibull distribution. For the combined importance sampling and antithetic variates, termed IS-AV, the time-to-failure and time-to-repair are induced by their Weibull distributed random variables, which are related to their respective pair of complementary random seeds as shown in (4-18) and (4-19).

The algorithm outlined in Fig. 4-1 using the conventional method ends up with 1.69% coefficient of variation over 250 simulation years. The IS and the IS-AV methods are executed until the same coefficient of variation are achieved.

Fig. 4-3 and 4-4 show the convergence of the EENS. The IS method requires 82 simulation years, while the IS-AV approach only requires 65 simulation years for the same convergence criterion. Therefore, the speedup ratios of these two approaches compared to the conventional one are

$$Speedup_{IS} = 250/82 = 3.05\ , \tag{4-23}$$

$$Speedup_{IS-AV} = 250/65 = 3.85\ . \tag{4-24}$$

Note that they are much higher than those of the antithetic variates algorithm given in [6]. The exact computing time is not specified here because the program developed here has not yet been optimized.

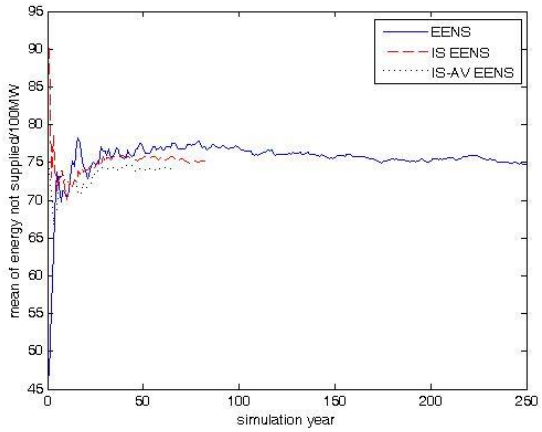

Fig. 4-3 EENS comparison between the conventional,
the IS, and the IS-AV algorithm for the IEEE one-are RTS.

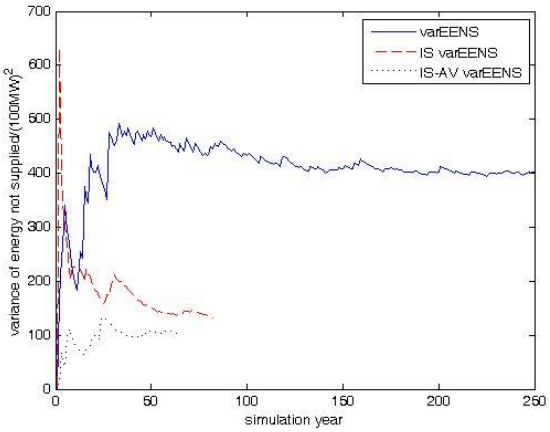

Fig. 4-4 EENS variance comparison between the conventional,
the IS, and the IS-AV algorithm for the IEEE one-area RTS.

TABLE 4-1
EENS comparison between the conventional, the IS, and the IS-AV algorithm
for the IEEE one-area RTS when $C_v = 1.69\%$.

	Conventional method	IS method	IS-AV method
EENS ($\times 10^3 MWh$)	7.4757	7.5141	7.4245
Difference %	0	0.50	0.69
Simulation years	250	82	65
Speedup ratio	0	3.05	3.85

The final data results are provided in Table 4-1. They show that the importance sampling algorithm noticeably outperforms the conventional method while the combined method outperforms the simple importance sampling approach to a certain extent. In addition, the correlated variates approach has been implemented as proposed in [6]. This method has resulted in no obvious variance reduction on the IEEE one-area RTS. The reason is that the correlation between the estimation target and auxiliary random variable is too small to reduce the variance of the EENS estimate.

4.6.2 Case II – IEEE three-area RTS

The IEEE three-area RTS consists of three IEEE one-area RTS, which have 96 generating units with a total installed capacity of 10,215 MW. There are 73 buses connected by 120 transmission lines in the system. In order to decrease the computational burden, the daily load is roughly divided into three average time intervals, namely, peaking time, base load time, and intermittent time. Since the evaluation is launched for long-term planning, it is reasonable to set the time unit of the simulations as eight hours. The simulation procedure is identical to that shown in Fig. 4-1 except for the time unit of the simulations and for all the loads.

The conventional method is also executed for 250 simulation years with a 1.95% coefficient of variation. The IS and the IS-AV methods are executed until the same values of the coefficients of variation are achieved.

The convergence of the EENS is shown in Fig. 4-5 and 4-6. The IS method requires 124 simulation years while the IS-AV approach requires only 110 simulation years for the same convergence criterion. Therefore, the speedup ratios of these two approaches compared to the conventional one are

$$Speedup_{IS} = 250/124 = 2.02\ , \tag{4-25}$$

$$Speedup_{IS-AV} = 250/110 = 2.27\ , \tag{4-26}$$

which are noticeable although smaller than those obtained on the IEEE one-area RTS.

The final data is provided in Table 4-2 for both the IS and IS-AV methods. It is observed that the importance sampling algorithm noticeably outperforms the conventional method. Compared to the simple importance sampling algorithm, the combined IS-AV approach provides minor improvement, because of the limited impact that the time-to-failure and time-to-repair have on the variance of the EENS.

As for the biases of the EENS calculated using the IS-AV and the IS method and shown in Table 4-1 and 4-2, they increase slightly for the 73-bus IEEE three-area RTS system as compared to the 24-bus IEEE one-area RTS system. Specifically, while being smaller for the IS-AV than for the IS, they exhibit a growth rate of 1.58 for the former versus 5.86 for the latter. From these results, it is conjectured that they will continue to grow as system size increases further. Additional simulations are required to check whether they remain within an acceptable range.

Regarding the transmission line outages, an algorithm implementing the antithetic variates method has been applied to them. As expected, the results show almost no improvement due to the non-monotonic relationship between the state of transmission lines and the estimation index.

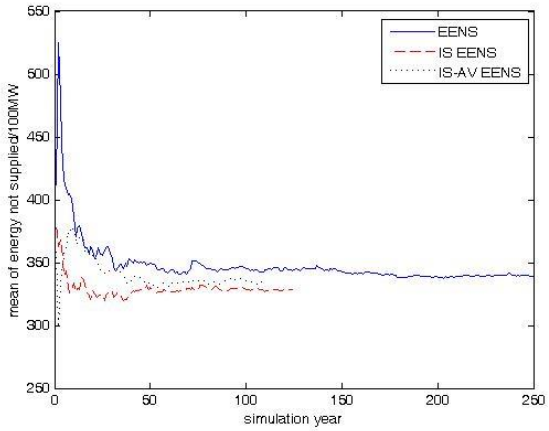

Fig. 4-5 EENS comparison between the conventional, the IS, and the IS-AV algorithm for the IEEE three-area RTS.

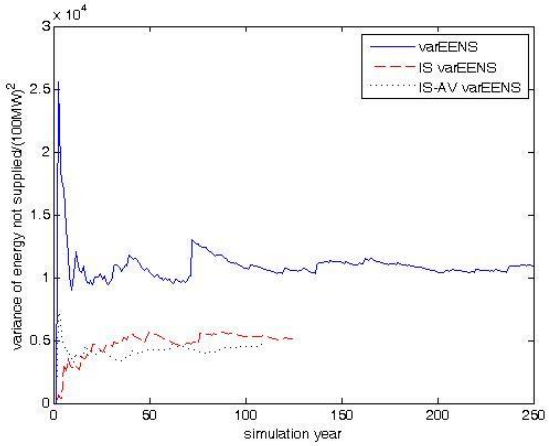

Fig. 4-6 EENS variance comparison between the conventional, the IS, and the IS-AV algorithm for the IEEE three-area RTS.

TABLE 4-2
EENS comparison between the conventional, the IS, and the IS-AV algorithm for the IEEE three-are RTS when $C_v = 1.95\%$.

	Conventional method	IS method	IS-AV method
EENS ($\times 10^4 MWh$)	3.3886	3.2894	3.3518
Difference %	0	2.93	1.09
Simulation years	250	124	110
Speedup ratio	0	2.02	2.27

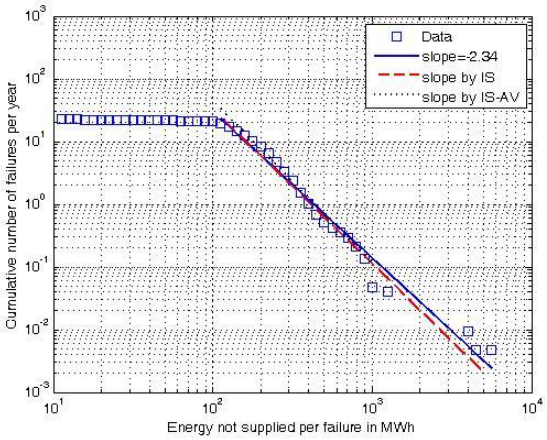

Fig. 4-7 Log-log plots of the cumulative number of failures per year vs. the energy not supplied in MWh between the conventional Monte Carlo method, the IS, and the IS-AV procedures. The slope of the linear segment of the plot for the conventional Monte Carlo method is -2.34. The slopes for the IS and IS-AV are -2.47 and -2.58, respectively.

To test whether the yearly energy-not-served per failure follows a power-law distribution, the statistical tests proposed in [44] are applied to the recorded data displayed in a log-log scale plot shown in Fig. 4-7. The authors of [44] mention three alternative probability distributions that may result in a linear decrease for large values of the random variable under study. These are the exponential, the log-normal and the power-law distributions. All three distributions have been tested, yielding the following results. The Kolmogorov-Smirnov test rejects the exponential distribution as a possible candidate with a value of

0.412 versus 0.093 and 0.095 for the other two distributions. On the other hand, the likelihood ratio test clearly points to a power-law distribution as a better model with a value of -2.5 against -229.9 for the log-normal distribution. Therefore, it is concluded that power law distributions have been obtained for all three sequential Monte Carlo methods involving cascading failures with a slope of -2.34 for the conventional method and slightly more negative slopes for the IS and IS-AV techniques.

From Fig. 4-7, it is observed that the majority of the ENS values are associated with the left flat segment of the log-log plot of the cumulative number of failures. The tail of that plot follows a power-law distribution, which demonstrates that the occurrence of severe blackouts is rare with extremely large ENS values. The similarity of the slopes of the three methods depicted in Fig. 4-7 reveals that the ENS distributions of the IS and IS-AV methods are close to the one of the conventional method while the associated numbers of trials differ.

4.7 Conclusion

A risk-based composite power system vulnerability evaluation has been developed. Unlike conventional methods, it models cascading failures in power transmission networks due to various mechanisms observed in actual blackouts, including relay over-tripping, short-circuits due to overgrown trees, voltage sags, to cite a few. Since cascading failures involve sequences of dependent outages, a sequential Monte Carlo simulation approach has been used.

To reduce the computational burden while maintaining the accuracy of the results at a given level, two variance reduction techniques have been applied, namely, the IS and the IS-AV approach. Both the IEEE one-area RTS and the IEEE three-area RTS are utilized to assess the performance of these two algorithms. The simulations conducted here have shown that the performance of the IS-AV approach exceeds the simple IS algorithm to a certain extent. However, while both the IS and the IS-AV algorithms are able to noticeably reduce the number of samples that need to be executed on both IEEE RTSs, their relative efficiencies are very much model dependent.

Chapter 5

Optimal Placement and Sizing of Microgrids in Composite Reliability of a Deregulated Power System

5.1 Introduction

Power system planning is undergoing a transition towards probabilistic approaches due to, among other things, deregulation and interconnection of microgrids triggered by public concerns regarding rising electric energy costs, more frequent power outages, limited fossil fuel resources, and increasing environmental air and water pollution, to cite a few [3]. Microgrids, which are small-scale networks interconnecting distributed generation (DG), storage devices, loads and converters, are evolving thanks to technological advancements.

While to our knowledge, there is no paper on optimal placement and sizing of microgrids in a bulk power system for reliability enhancement, there is a growing literature dealing with the placement of DGs in power distribution systems or the impact on distribution system reliability. For instance, Hedayati *et al.* [47] initiate a method for placement of DG units by installing DGs at the most sensitive buses to system voltage collapse with the execution of Continuous Power Flow (CPF) programs. In addition to selecting the DG location via CPF, Yuan *et al.* [48] advocate the use of a primal-dual interior point method to solve the optimal reactive power output of DGs. For the improvement of the voltage profile, Arief *et al.* [49] propose to install DGs at buses with high modal participation factors in Q-V sensitivity analysis.

Other researchers formulate the objective of DG penetration as the minimization of the active power loss in the distribution system [50], [51]. Another DG sizing approach advocated by Nekooei *et al.* [52] consists in applying multi-objective optimization that involves both network power loss minimization and voltage regulation maximization. Kumar *et al.* [53] set the objective as social welfare maximization where DGs are treated as regular generators and where the optimal DG placement is governed by the cost characteristics of DG and central generations. Here a deregulated power system is considered where the DG costs and social welfare are taken into account.

In most of the current power markets, the wholesale electricity purchases and sales are settled based on Locational Marginal Prices (LMPs). LMP is defined as the marginal cost of serving the next increment electric load at a specific location [75]. The standard LMP consists of three components, namely, marginal energy component, marginal congestion component, and marginal loss component. The former two components are reflected in the optimization results of the total electricity purchasing cost minimization while the last one can vary.

There is also a literature on the reliability evaluations of distribution systems with DGs [58-59] or of microgrids, which are characterized by a variety of structures and topologies [60-61]. Other literature deals with the optimal sizing and the placement of DGs within a microgrid to improve its reliability [54-56], [63-64]. Specifically, Vallem *et al.* [54] and Basu *et al.* [55] propose an approach that first minimizes the deployment cost or system losses and then evaluates the reliability of the power distribution system. Gantz *et al.* [56] improve distribution system reliability by minimizing the aggregate cost of all customers' outages during a given outage period. Arefifar *et al.* [62] achieve microgrid reliability enhancement by optimizing the location of switches.

Using Monte Carlo simulations based on importance sampling and antithetic variates, Chen and Mili [66] assess the risk of cascading failure in composite power system reliability due to relay overtripping, overgrown vegetation, and voltage collapse. In contrast, in this chapter the impacts of microgrids on composite power system reliability are analyzed using sequential Monte Carlo simulations. The developed algorithm seeks an optimal placement and sizing of microgrids responding to LMPs in a deregulated environment. The placement and size of microgrids are initially set up based on voltage participation factors calculated from the reactive power Jacobian matrix. The modeling of microgrids is carried out for two operation modes, namely, grid-connected and islanded mode. To reduce the computational burden of the simulations, the control strategy proposed in Khodayar *et al.* [57] is not applied for optimal microgrid operation in distribution systems. Rather a simplified model for microgrids is assumed, each represented as a collection of renewable energy generation units, micro-turbines, and storage devices that are coordinated by a heuristic optimization algorithm.

Upon completion of the Monte Carlo simulations, a quadratic programming algorithm is executed. It provides a collection of optimal solutions of microgrid placement and sizing for various abnormal states of the system. By resorting to cluster analysis and the least-squares method, a single final solution is identified as representative of the largest cluster of candidates. To evaluate the proposed approach, two case studies are carried out on the Roy Billinton Test System (RBTS) and the IEEE Reliability Test System (RTS). Simulation results show that for both power systems, a small penetration of 5% of

microgrids induces a significant improvement of system reliability while decreasing the risk of cascading failure.

This chapter is organized as follows. Section 5.2 investigates four issues raised by connecting microgrids to the main grid. Section 5.3 describes the implementation of Monte Carlo modeling with embedded microgrids. Section 5.4 presents an optimal placement and sizing method of microgrids for system reliability enhancement. Section 5.5 describes two-case studies on RBTS and IEEE RTS. The conclusions and some future work are outlined in Section 5.6.

5.2 Impacts of Microgrid Penetration on System Vulnerability

In this section, an overview of the various issues raised by microgrid operation and control in both islanded and grid-connected mode of operation is provided.

5.2.1 Voltage Control Using Microgrids

Microgrids are connected at different locations along radial distribution feeders. Depending on the size and location of the distributed generators within the microgrids, it is possible to control the voltage at the point of interconnection with the main grid. However, a small-scale microgrid may not be able to regulate its bus voltage if its reactive power supply is insufficient [65]. Therefore, microgrid buses are divided into two types, namely PQ or PV buses that respectively connect small-scale and large-scale microgrids.

5.2.2 Energy Storage within Microgrids

In addition to loads, microgrids encompass energy sources such as wind or solar generation, fuel cells, and a variety of energy storage devices, including fly-wheels, heat pumps, and electric vehicle batteries, which have the ability to mitigate the intermittency of the renewable energy resources. To optimize the operation of the batteries, an economic scheduling that accounts for their capacity and charging/discharging cycles is carried out. Thanks to these features, microgrids exhibit many beneficial effects on power system operation and control, which include decreasing peak load demand in normal conditions and supplying reserve in abnormal conditions, among other things.

5.2.3 Transmission Loading due to Microgrids

Microgrids can serve a rural village far from the backbone of the main grid or an incremental urban load far from generation buses. Unlike traditional power system planning for which new generators and transmission lines are added to balance additional loads, microgrid integration does not require the addition of a significant amount of transmission capacity since the new load is served locally. Consequently, transmission losses and congestions are decreased. Because line and transformer overloading is one of the main reasons of cascading failure propagation, the penetration of microgrids mitigates the risk of such events as shown next.

5.2.4 Independent Operation of Microgrids

From the viewpoint of local load, a microgrid can be considered as a back-up generator in case of system contingencies. Indeed, with its multiple DGs and energy storage devices, a microgrid may serve partially or totally its own load while operating in an islanded mode. Consequently, during or in the aftermath of a blackout, the loss of load incurred by a power system with interconnected microgrids is diminished.

5.3 Monte Carlo Modeling of System Operation with Microgrid Integration

Sequential Monte Carlo simulations are implemented to account for all possible real system scenarios of cascading failure. It accounts for microgrid operation aimed at achieving both economic dispatch and system reliability enhancement.

5.3.1 Overview of Monte Carlo Modeling Considering Cascading Failures

Since system failures may cascade in numerous ways, sequential Monte Carlo simulations for power system reliability analysis are performed in a number of plausible scenarios. Here, the state duration approach is implemented, where operating and repair state durations are assumed to be exponentially distributed. Other components and devices are modeled, including over- and under- voltage relays on generators and large-capacity motors, zone-3 impedance relays on transmission lines, and vegetation under transmission lines. Since the actions of these components hinge on system power flow and nodal voltage patterns, the simulations require the execution in hourly increments of full AC power flow calculations. A DC Optimal Power Flow (DC OPF) algorithm is also executed for economic dispatch evaluation and load shedding determination in abnormal operating conditions.

The approach used here for modeling system restoration has been inspired by the work of Hou *et al.* [36] and Ozog *et al.* [37], who have independently shown that the energy not supplied exhibits a linear growth with ups and downs as the restoration time increases. This prompts the modeling of the energy not supplied as a straight line segment starting from the origin and ending at the total load demand over a period of 4 hours. More detailed information about the model is provided in [66].

5.3.2 Operation and Control of Microgrids

In the simulations, the operation of the embedded microgrids requires the optimal coordination of three basic energy resources, namely renewable energy, energy storage and micro-turbine generation. Since the operating costs of renewable energy resources, such as wind or solar devices, are much lower than those of fuel-based generating unit, their operation does not depend on that of the energy storage and the micro-turbines of a microgrid. Therefore, the operating cost of the renewal energy sources may be assumed to be zero for convenience. In normal conditions, energy storage devices achieve peak load shaving and valley load filling, while in abnormal conditions they provide their maximum energy to support the main grid if the latter is still remediable. Since micro-turbines operate with fuel consumption, which has a cost, their output is determined by Locational Marginal Prices (LMPs). However, this rule does not apply during abnormal conditions because LMPs may not exist. During these conditions, micro-turbines are required to serve critical loads.

An economic operation of a microgrid aims at maximizing its profits defined as the income from selling electric energy to the main grid minus the cost of purchasing it from the grid and the operating cost of the micro-turbines that it encompasses. This leads to the optimization problem expressed as

$$\max \sum_{i=1}^{T} \left(E_i^{RE} + E_i^{ES} + E_i^{MT} - E_i^{Load}\right) LMP_i - c^{MT} E_i^{MT} , \qquad (5\text{-}1)$$

where T is the number of scheduled hours; c^{MT} is the cost of micro-turbine operation per kWh; E_i^{RE}, E_i^{ES}, E_i^{MT} are respectively the energy output from the renewable energy generators, the energy storage devices, and the micro-turbines located within the microgrid in the ith hour; E_i^{Load} is the load consumption in the microgrid at the same hour. Here, the locational marginal price, LMP_i, is calculated by executing a DC OPF program, the inputs of which include the costs of generating units. For simplicity, the system loss component in LMP is ignored and the energy storage efficiency is assumed to be one.

This optimization problem is subject to several constraints, which are given by

$$E_i^{TES} = \sum_{j=1}^{i} E_j^{ES}, \quad (5\text{-}2)$$

$$-R_{max}^{Ch} \leq E_i^{ES} \leq \min(E_{i-1}^{TES}, R_{max}^{Dch}), \quad (5\text{-}3)$$

$$0 \leq E_i^{TES} \leq C^{ES}, \quad (5\text{-}4)$$

$$0 \leq E_i^{MT} \leq C^{MT}, \quad (5\text{-}5)$$

where E_i^{TES} is the total energy stored in the energy storage devices in the ith hour; R_{max}^{Ch} and R_{max}^{Dch} are respectively the maximum charging and discharging rates of the energy storage devices; C^{ES} and C^{MT} are respectively the capacities of the energy storage devices and of the micro-turbines located within microgrids.

Unfortunately, it is very difficult to perform an optimal coordination of the microgrid components every hour over a long term horizon, e.g. one year. One reason for this is the existence of a very large number of variables to be optimized, which can only be achieved by means of a time consuming optimal programming iterative algorithm. Another reason is the infeasibility of the OPF that calculates the LMPs under abnormal sates, which are characterized by either the deficiency of the generation supply to the load demand, or the ill-conditioning, or the singularity of the Jacobian matrix.

Before the power system transitions to an abnormal state, microgrids should be preparing for the worst, for example charging their batteries to their maximum capacity. Therefore, a short-term coordination optimization of their operation should be performed in each hour over the next 24 hours. There are three main reasons for executing this optimization plan. Firstly, a load profile typically includes peaks and valleys that cycle every 24 hours. So the LMP profile has similar 24-hour cycles. Secondly, the 24 hours are longer than a complete minimum charging and discharging cycle of commonly used lithium-ion and lead-acid batteries. Thus, an optimal schedule of a battery cycle is possible. The characteristics of this type of batteries, as given in [67], are displayed in Table 5-1. Here,

Table 5-1
Lithium-ion, lead-acid battery characteristics [67]

Item	Value	Unit
Capacity	50	kWh
Power	25	kW
Max Charging Rate	12.5	kW/h
Max Discharging Rate	25	kW/h

the minimum charging and discharging cycle is 6 hours. Lastly, in each hour, an optimization is achieved over the next 24 hours using the forecasted load demand and the predicted output of the renewable energy sources so that any system state change (e.g. a generation unit drops or a line trips) in any hour could be updated for the next 24-hour optimization.

Instead of solving for the optimal values of the variable set $\{E_i^{ES}, E_i^{MT}, E_i^{TES}\}$ for each hour of a day, we calculate one set of values for the current hour given the predicted E_i^{Load} and E_i^{RE} for the next 24 hours. Assuming that the same system components remain in service over a day, two scenarios are defined as follows:

Scenario 1: The system is assumed to settle in a normal state over a 24-hour period, which allows us to calculate the LMPs during that period using an OPF. From the current hour to the 24th hour, the energy storage devices are charged to their maximum capacity at their maximum charging rate when the LMPs are at their lowest values. The charging energy is obtained from the remainder of the renewable energy once the local load in the microgrid is supplied. If the remainder is insufficient, the microgrid buys the missing energy from the main grid. Then the energy storage devices are discharged during the hours where the LMPs are at their highest values. Note that the discharged energy is limited to a maximum value equal to the previously total stored energy. For the remaining hours, a microgrid purchases or sells the difference between its generated renewable energy and its local load whereas its micro-turbine generation is dependent only on the LMPs.

Scenario 2: The system is assumed to settle in an abnormal state over a 24-hour period. For the hours before the first predicted abnormal state where an optimal solution cannot be obtained from the LMP OPF, the energy storage devices are charged as in Scenario 1. Then, from the hour just before the abnormal hour up to the current hour, the energy storage devices are charged to their maximum capacity. The charging energy is first made from the grid and then from the micro-turbines if necessary. Note that the micro-turbines may be forced to run in order to charge the energy storage devices regardless of the values of the LMPs.

In each simulation hour, the microgrid supplies/absorbs energy to/from the main grid. The instant reserve capacity that the microgrid exchanges with the main grid depends on the remaining power output capacity of the micro-turbines and the maximum discharging ability of the energy storage devices, given their current stored energy after optimal coordination. When any other abnormal conditions occur in the system, for instance system reserve is too small, or negative, or the power flow program does not converge, the instant reserve energy is added to the output energy of the microgrids.

The developed Monte Carlo simulation procedure is briefly summarized in Fig. 5-1. The subroutine entitled "Microgrid Component Coordination" is carried out for both a normal and an emergency scenario as described in Scenario 1 and 2, respectively. This subroutine yields the scheduled power output and the instant reserve capacity that a microgrid provides to the main grid. These are in turn used as the input data and as the power output constraints in the subsequent power flow and DC OPF subroutines. The latter subroutine involves a load-shedding function when the power system is still insecure once the microgrid reserves are exhausted. The details are provided next.

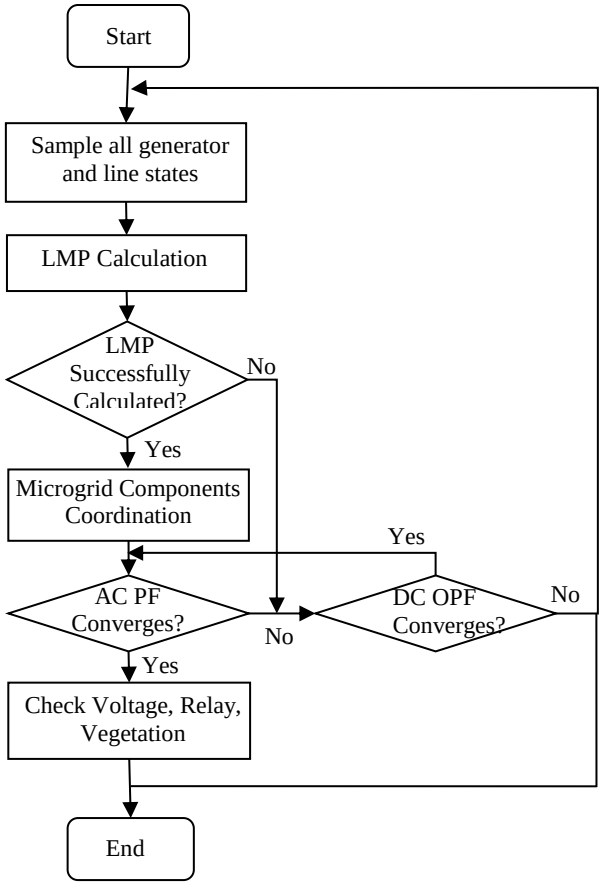

Fig. 5-1 Flowchart of the developed Monte Carlo algorithm.

5.4 Optimal Placement and Sizing of Microgrids

This section describes the entire process, from the initial steps of the Monte Carlo simulations to the final step that results in the optimal solution for system reliability enhancement. It consists of generating numerous system state scenarios as described in the previous section. Note that because microgrids affect composite reliability

exclusively during abnormal states, the optimization procedure for microgrid placement and sizing is executed only during these states.

5.4.1 Initial Placement of Microgrids Using Modal Analysis

The sequential Monte Carlo simulation starts with a set of initial input data, including the locations and sizes of microgrids. In this paper, the initial microgrid placement is assigned based on voltage sensitivity analysis.

The linearized power flow equation is given by

$$\begin{bmatrix}\Delta \boldsymbol{P} \\ \Delta \boldsymbol{Q}\end{bmatrix} = \begin{bmatrix}\boldsymbol{J_{P\theta}} & \boldsymbol{J_{PV}} \\ \boldsymbol{J_{Q\theta}} & \boldsymbol{J_{QV}}\end{bmatrix}\begin{bmatrix}\Delta \boldsymbol{\theta} \\ \Delta \boldsymbol{V}\end{bmatrix}, \tag{5-6}$$

where the power flow Jacobian matrix consists of four sub-matrixes, namely $\boldsymbol{J_{P\theta}}$, $\boldsymbol{J_{PV}}$, $\boldsymbol{J_{Q\theta}}$, and $\boldsymbol{J_{QV}}$. If $\Delta \boldsymbol{P} = \boldsymbol{0}$, it results

$$\Delta \boldsymbol{Q} = \left[\boldsymbol{J_{QV}} - \boldsymbol{J_{Q\theta}}\boldsymbol{J_{P\theta}^{-1}}\boldsymbol{J_{PV}}\right]\Delta \boldsymbol{V}. \tag{5-7}$$

The reduced Jacobian matrix J_R is defined as

$$\boldsymbol{J_R} = \boldsymbol{J_{QV}} - \boldsymbol{J_{Q\theta}}\boldsymbol{J_{P\theta}^{-1}}\boldsymbol{J_{PV}}, \tag{5-8}$$

and its eigen-decomposition is given by

$$\boldsymbol{J_R} = \boldsymbol{\Phi\Lambda\Psi}. \tag{5-9}$$

Here $\boldsymbol{\Phi}$ is the right eigenvecter matrix, $\boldsymbol{\Psi}$ is the left eigenvector matrix, and $\boldsymbol{\Lambda}$ is the eigenvalue matrix. If the real-part of the ith eigenvalue in $\boldsymbol{\Lambda}$, λ_i, is positive, then the ith voltage mode varies along the same direction as the ith reactive power mode, indicating that the system exhibits voltage stability. If the real-part of λ_i is negative, then the ith voltage mode varies in the opposite direction of the ith reactive power mode, indicating that the system exhibits voltage instability. In that case, the ith voltage mode becomes unstable as the positive real part of λ_i gets close to 0 [76].

The kith participation factor is defined as

$$p_{ki} = \Phi_{ki}\Psi_{ik}. \tag{5-10}$$

It indicates the sensitivity of the ith eigenvalue to the reactive power injection of Bus k. Here, the initial state of the power system is assumed to be stable, which implying that a power flow solution may exist. N_{MG} buses with the largest participation factors corresponding to the eigenvalue that has the smallest real part for microgrid placement

are selected because they reflect the largest contribution of the reactive power injection of these buses to the weakest voltage stability mode [49]. The initial sizes of these microgrids are picked proportional to these participation factors.

5.4.2 Optimal Sizing of Microgrids

During the simulations carried out for system reliability evaluation, microgrids contribute to system reliability only when the system is in abnormal states as featured in the DC-OPF subroutine displayed in Fig. 5-1. This subroutine seeks the optimal sizing of microgrids as a solution to the following optimization problem:

$$min\{\sum_{i=1}^{N} C_{Gi}P_{Gi} + \sum_{i=1}^{N} C_{Li}P_{Li} + \sum_{i=1}^{N_{MG}} C_{MG}P_{MGi} + PF_{MGi}\}, \quad (5\text{-}11)$$

subject to

$$\sum_{MGi=1}^{N_{MG}} P_{MGi} \leq Total\ Microgrid\ Capacity, \quad (5\text{-}12)$$

$$\sum_{i=1}^{N} P_{Gi} + \sum_{i=1}^{N} P_{Li} + \sum_{MGi=1}^{N_{MG}} P_{MGi} = \sum_{Li=1}^{N} P_{Di}, \quad (5\text{-}13)$$

$$|\boldsymbol{F}| \leq \boldsymbol{F_{max}}, \quad (5\text{-}14)$$

$$\boldsymbol{P_{G,min}} \leq \boldsymbol{P_G} \leq \boldsymbol{P_{G,max}}, \quad (5\text{-}15)$$

$$\boldsymbol{0} \leq \boldsymbol{P_L} \leq \boldsymbol{P_D}, \quad (5\text{-}16)$$

where

P_{Gi} is the power output of generation Bus i;
$\boldsymbol{P_G}$ is the generation power output vector;
P_{Li} is the amount of load curtailment at load Bus i;
$\boldsymbol{P_L}$ is the load curtailment vector;
P_{MGi} is the real power generation at microgrid Bus MGi;
P_{Di} is the demand power at load bus i;
$\boldsymbol{P_D}$ is the power demand vector;
$\boldsymbol{F}$ is the real power flow vector;
$\boldsymbol{F_{max}}$ is the real power flow upper limit vector;
$\boldsymbol{P_{G,min}}$ is the generation power lower limit output vector;
$\boldsymbol{P_{G,max}}$ is the generation power upper limit output vector;
PF_{MGi} is the penalty function at microgrid Bus MGi.

Here C_{Gi} denotes the actual marginal cost of the ith generation that is bid in an efficient power market while C_{Li} denotes the marginal loss at load Bus i; it indicates the importance of the curtailed load at that bus. In fact, C_{Gi} and C_{Li} represent the priority

order among the traditional power plant output and the load curtailment, respectively. The value of C_{Li} is difficult to evaluate in practice, but it is recommended to have $\min(C_{Li}) > \max(C_{Gi})$ for decreasing the amount of load shedding. As for C_{MG}, it does not have an actual physical meaning. However, it is worth mentioning that when the comprehensive cost of microgrids, accounting for microgrid installation and operation costs, is the same for all the candidate microgrid locations, C_{MG} is set to a fixed value between $\min(C_{Li})$ and $\max(C_{Gi})$. This value is chosen so that, when the system is in abnormal state, the optimal P_{MGi} will be the minimum power support that the system needs from the microgrid Bus i to guarantee its transition to the normal state initiated by the smallest load curtailment.

Since all the microgrid power outputs, $\{P_{MG1}, \dots, P_{MG,N_{MG}}\}$, share the same weight, C_{MG}, the optimization problem given by (11) may have multiple solutions for a given system state. To constrain the solution to be unique, a penalty function is assigned to each microgrid placement and sizing. For the microgrids Bus MGi, that function is expressed as a weighted squared difference between two real power output ratios defined as follows: the first ratio is that of the current power output of the *i*th microgrid to that of the microgrid in the system with the initial maximum power output while the second ratio is that of the initial power output, P_{MGi}^0, to the initial maximum power output of the *i*th microgrid, $max(P_{MGi}^0)$. Formally, it is expressed as

$$PF_{MGi} = a_{MGi}\left(\frac{P_{MGi}}{P_{MGm}} - \frac{P_{MGi}^0}{max(P_{MGi}^0)}\right)^2, \tag{5-17}$$

where

$$m = arg\max_{1 \le i \le N_{MG}}(P_{MGi}^0). \tag{5-18}$$

Note that if no transmission constraints are binding, the penalty function given by (5-17) reduces to zero at the optimal solution, and if some constraints are binding, a small value to the weight a_{MGi} is assigned so that the penalty function barely affects the optimal solution.

5.4.3 Statistical Analysis of the Optimal Solutions

During the simulations, when the optimal solution of the DC-OPF differs from the initial microgrid placement and sizing, it is counted as a microgrid candidate in the next step of the search. Note that because the simulation algorithm investigates many cases, a set of candidates are identified upon completion of this step.

The objective of the final step is to find the solution that improves the reliability the most from all the identified candidates. To this end, we first resort to a clustering algorithm that classifies the candidates into clusters. Then, we select a fraction of the largest clusters and find the best representative solution of each of them. Finally, we run the reliability evaluation simulations described in Section 3 using the identified representative solutions. The solution that improves the reliability index the most is the final optimal set of microgrid placement and sizing.

Let us provide the details of the foregoing procedure. First, let us emphasize that there is a constraint fixed by the investment budget, which is the total microgrid capacity. Therefore, the problem boils down to finding the optimal ratio between the capacities of the microgrids and their best placement to achieve the highest system reliability. Now, a microgrid placement and sizing candidate can be represented by a point identified by a vector in a N_{MG}-dimentional space. All the candidates form a point cloud in this space, typically organized in clusters. The distance between any pair of vectors in the same cluster must be short enough so that all members of one cluster have close contributions to system reliability. Because microgrid capacity ratios only relate with vector angles, not vector magnitudes, the distance between a pair of candidates is defined as the angle between the associated pair of vectors, which is given by

$$d(\boldsymbol{V_1}, \boldsymbol{V_2}) = \frac{\boldsymbol{V_1} \cdot \boldsymbol{V_2}}{\|\boldsymbol{V_1}\| \|\boldsymbol{V_2}\|}. \tag{5-19}$$

A simple but effective clustering algorithm is as follows:

Step 1: Randomly pick a vector as the center of the first cluster.

Step 2: Randomly pick another vector, then calculate the angle between this vector and the existing cluster centers and find the smallest one.

Step 3: If the shortest distance is within a given threshold, this vector is added as a new element to the closest cluster; if not, it becomes the center of a new cluster.

Step 4: Repeat Step 2 and 3 for all the remaining vectors.

After identifying all the clusters, the cluster representatives are calculated by minimizing the sum of the squares of the distances between this vector and the other vectors in the same cluster. Formally, it is expressed as

$$\boldsymbol{V_R} = arg\ \min_{\boldsymbol{V_i}} \sum_{\substack{j=1 \\ j \neq i}}^{N_S} d^2(\boldsymbol{V_i}, \boldsymbol{V_j}), \tag{5-20}$$

where N_s is the number of the vectors in cluster S. Other criteria, such as

$$\boldsymbol{V_R} = arg\ \min_{\boldsymbol{V_i}} \sum_{\substack{j=1 \\ j \neq i}}^{N_S} d(\boldsymbol{V_i}, \boldsymbol{V_j}), \tag{5-21}$$

have been applied to test whether the selected representative lies in the center of the associated cluster.

In the final step, reliability evaluations are carried out using the representatives of the top large clusters to get the final solution that improves the composite system reliability the most.

5.5 Simulation Results

The developed reliability evaluation method has been applied to a revised RBTS and the IEEE RTS, whose original data is respectively provided in [4] and [18]. For both systems, a microgrid penetration is assumed to be able to cover 5% of the system annual peak load. This is achieved by replacing an appropriate amount of conventional generating unit capacity by an equal amount of microgrid capacity. The initial condition for the simulations is a normal operating case of the system without any generator or transmission line outages. The average temperature data of the city of Falls Church in Virginia [19] is taken as the ambient temperature data, which plays a role in modeling the vegetation growth rate in the simulations.

Each microgrid consists of 4 energy blocks, namely load, renewable energy, energy storage and micro-turbines, whose characteristics are given in Table 5-3. The power output of a renewable energy unit is assumed to follow a Beta distribution as in [68], with the maximum value equal to the peak load in the microgrid. The charging/discharging rates of the batteries installed as energy storage devices and the maximum power outputs of micro-turbines are all set to be proportional to the peak load as shown in Table 5-2.

Table 5-2
Energy sources in microgrids (% peak load)

Item	Renewable Energy	Energy Storage	Micro-turbine
Max power output	100	50	50
Capacity	-	200	-
Discharging Rate	-	25	-
Distribution	$Beta(4,4)$	-	-

5.5.1 Case I – Revised RTBS

The original RBTS has 11 generating units with a total installed capacity of 240 MW and has 6 buses connected by 9 transmission lines. In our simulations, the system peak load is increased from 185 MW to 200 MW. The total microgrid capacity amounts to 10MW, yielding a penetration level of 5%. A 10-MW generating unit on Bus 1 has been replaced by microgrid capacity. Because the original RBTS contains an obvious weak node at Bus 6, which is an antenna, an additional transmission line from Bus 6 to Bus 4 is added. It is on this revised RBTS that the simulations are carried out.

The proportions of the real power capacities of the microgrids connected to the four load buses of the system are equal to the corresponding voltage stability participation factors given by (5-10). As for their maximum reactive power capacities, they are assumed to be equal to twice the amounts of their real power capacities as indicated in [69]. Note that the reactive power capacities of Bus 3 and Bus 4 are not sufficient to regulate the voltages at these buses.

Sequential Monte Carlo simulations involving cascading failure are executed on an hourly basis to evaluate over 100 simulation years the EENS of the revised RBTS without microgrids. Then a second series of simulations are performed where a microgrid placement and sizing optimization is carried out, yielding 62 optimal microgrid placement candidates. By setting $\cos^{-1} 0.95$ as the threshold for cluster determination, 8 clusters are formed. The three largest clusters cover more than 10% of the total number of candidates. The proportions of their representatives are used in the simulations for reliability evaluation. These simulations are labeled as Microgrid-Embedded Case 2, 3, and 4 in Table 5-3.

The simulation results displayed in Table 5-3 reveal that the EENSs of all the microgrid-embedded cases are significantly smaller than those of the conventional case without microgrids. Since the smallest EENS comes from Microgrid-Embedded Case 3, its microgrid capacity proportion is the final optimal microgrid placement and sizing solution. Regarding system reserve capacities and transmission losses of the microgrid-embedded cases, it is observed that they have not improved since the transmission maximum loading level has decreased and the average loading level has slightly increased. This is due to the small microgrid penetration level chosen to be 5% of the system peak load. Note that the main objectives set up as the enhancement of system reliability along with the decrease of the number of cascading failures have been met. The number of cascading failure is relatively small even in the conventional case due to the limit number of simulation years being performed, the load shedding mechanism being executed in the simulation, and the robustness of the IEEE RTS itself.

Table 5-3
Comparison between the conventional case and five microgrid-embedded cases for RBTS

		Conventional Case	Microgrid-Embedded Case 1[1]	Microgrid-Embedded Case 2	Microgrid-Embedded Case 3	Microgrid-Embedded Case 4
Microgrid capacity proportion	**Bus 3**	-	0.1101	0	0.1881	0
	Bus 4	-	0.2191	0.5263	0.3723	0
	Bus 5	-	0.2813	0.2368	0.2139	0
	Bus 6	-	0.3895	0.2368	0.2257	1
Cluster sizes[2]		-	-	37.10%	29.03%	17.74%
EENS (MWh)		139.9	51.31	85.62	45.66	64.62
ASRC[3] (MW)		108.1	110.0	93.1	110.2	95.83
ATL[4] (MW)		3.86	3.70	4.03	3.71	3.94
ATLMLL[5]		47.62%	46.25%	44.71%	46.25%	44.37%
ATLALL[6]		24.83%	25.36%	26.93%	25.50%	25.91%
NCF[7]		3	0	0	0	0

Table 5-4
Comparison between the conventional case and five microgrid-embedded cases for IEEE-RTS

		Conventional Case	Microgrid-Embedded Case 1[1]	Microgrid-Embedded Case 2	Microgrid-Embedded Case 3	Microgrid-Embedded Case 4	Microgrid-Embedded Case 5
Microgrid capacity proportion	**Bus 3**	-	0.1326	0	0	0	0.5035
	Bus 4	-	0.1665	0	0	1	0
	Bus 5	-	0.1093	1	0	0	0
	Bus 6	-	0.3173	0	0	0	0
	Bus 9	-	0.1132	0	1	0	0.4965
	Bus10	-	0.1611	0	0	0	0
Cluster sizes[2]		-	-	21.77%	31.65%	12.70%	14.11%
EENS $(\times 10^3 MWh)$		5.712	1.343	2.319	1.241	1.405	1.152
ASRC[3] $(\times 10^3 MW)$		1.386	1.470	1.406	1.458	1.473	1.459
ATL[4] (MW)		48.43	44.73	36.89	48.17	45.46	47.83
ATLMLL[5]		84.80%	78.19%	82.17%	83.30%	82.08%	82.74%
ATLALL[6]		26.84%	25.48%	22.30%	26.25%	25.40%	26.21%
NCF[7]		2	0	0	0	0	0

[1] The initial microgrid embedding case is labeled as Case 1.
[2] This is the number of elements in this cluster over the total number of candidates.
[3] This is the time average of system reserve capacity.
[4] This is the time average of transmission loss.
[5] This is the time average of transmission line maximum loading level.
[6] This is the time average of transmission line average loading level.
[7] This is the number of cascading failures over 100 simulation years.

5.5.2 Case II – IEEE RTS

The IEEE one-area RTS that was published in 1996 has 32 generating units with a total installed capacity of 3405 MW and has 24 buses connected by 38 transmission lines. The total microgrid capacity amounts to 142.5 MW, yielding a penetration level of 5%. The same amount of generation capacity on Bus 13 has been removed.

Based on the voltage stability participation factors given by (5-10), six load buses with the participation factors larger than 5% are selected as the microgrid placement candidate locations. The proportions of the capacities of the microgrids connected to the identified six load buses are equal to those of these participation factors. Sequential Monte Carlo simulations are carried out on the 24-bus IEEE-RTS system without and with microgrids.

Upon convergence, the simulations yield 496 optimal microgrid placement candidates, which are grouped in 18 clusters. Note that while the number of candidates and clusters for this system is significantly larger than those for the 6-bus RBTS, the number of the largest clusters that cover more than 10% of the candidates is identical. Similarly, the proportions of their representatives are used in the simulations for reliability evaluation. These simulations are labeled as Microgrid-Embedded Case 2 to 5 in Table 5-4.

From Table 5-4 it is observed that the EENSs of all the microgrid-embedded cases decrease significantly compared to the conventional case without microgrids. Microgrid-Embedded Case 5 provides the smallest EENS; therefore, its microgrid capacity proportion is the final optimal microgrid placement and sizing solution. Note that the EENSs of all except the Microgrid-Embedded Case 2 do not differ very much.

5.6 Conclusions

In this paper, we have developed a method for microgrid optimal placement and sizing in composite reliability of a deregulated power system involving cascading failures. The method consists of two main steps. Firstly, we execute a sequential Monte Carlo simulation while optimizing microgrid placement and sizing for the system abnormal states. A set of optimal candidates are generated using a clustering method and their representatives selected. By testing these representatives via reliability evaluation simulations, the final optimal solution is identified. The simulations on two test studies have shown that a small penetration of 5% of microgrids can lead to a significant improvement in reliability.

Chapter 6

Conclusions and Future Work

In this research work, an investigateion the propagation of cascading failures in 2003 U.S.-Canada Blackouts has been carried out. For the risk management of such massive blackouts, a risk-based composite power system vulnerability evaluation method is developed. The proposed model simulates cascading failures in power transmission networks due to various mechanisms observed in actual blackouts, including relay over-tripping, short-circuits due to overgrown trees, voltage sags, to cite a few. A sequential Monte Carlo simulation approach has been used because it can reflect the sequences of dependent outages.

The implementation of sequential Monte Carlo simulations entails a heavy computational burden in maintaining the accuracy of the results at a given level. We make use of two variance reduction techniques, namely the IS and the IS-AV approach, to alleviate this burden. Our simulations on two test systems have shown that the performance of the IS-AV approach exceeds the simple IS algorithm to a certain extent. However, while both the IS and the IS-AV algorithms are able to noticeably reduce the number of samples that need to be executed on both IEEE RTS, their relative efficiencies are very much model dependent.

Furthermore, the operation of microgrids interconnected with a power system is modeled to evaluate their impacts on composite system reliability. By optimally coordinating three types of microgrid energy sources, our simulation results show that microgrids connected to a power system provide more reserve energy and enhance system reliability significantly compared to the system without microgrids.

Furthermore, to maximize the reliability improvement of microgrid penetration, we have developed a method for microgrid optimal placement and sizing in composite deregulated power system subject to cascading failures. While using a sequential Monte Carlo simulation, the proposed method firstly optimizes microgrid placement and sizing for system abnormal states. This process generates a number of optimization results associated with different system abnormal states. Then by using a clustering method, the

representatives of the optimal candidates are selected. After testing these representatives, the final optimal solution is identified. The case studies have shown that a small penetration of 5% of microgrids can lead to a significant improvement in reliability.

6.1 Resilience Metrics [70]

Power system reliability has been an active research topic for a long time. Many methods have been developed and adopted by electric power utilities for power system planning purpose. These methods and algorithm have allowed power system to achieve a very high level of reliability when they are subject to disturbances. However, the risk of major disturbances that may induce large-scale blackouts threats the society and the economy. All the major blackouts, including the 2003 U.S.-Canada blackout and the two 1996 California blackouts, were very costly, in the billions of dollars of losses. With the development of advanced control and smart protection devices, interconnected via wide-area communications network, power systems may become more able to cope with major unexpected disturbances exhibiting an enhanced resiliency.

Mili [70] defines resilience as follows: "resilience to a class of unexpected failures is defined as the ability of a system to gracefully degrade and to quickly self-recover to a normal state". So the next question raised up is how to assess the resilience in engineering application. The third RESIN workshop held in Champaign in 2011 has proposed a framework for resilience metrics, which is utilized to suit critical infrastructures such as water, power, and transportation infrastructures. But it is necessary to explicit and practical metrics that can measure or estimate the resilience of power systems.

As pinpointed by Mili [70], there are two categories of resilience metrics from different standing points of utility grid and end users. In my opinion, utility grid's resilience metrics can be divided into two types based on their functions whether for prediction or for description, as shown in Table. 8-1. Predictive resilience metrics are utilized in grid planning to predict the risk of the existing or planned power system, while descriptive resilience are based on historical statistical data and are used for planning purpose.

6.1.1 Utility Grid's Resilience Metrics

Predictive resilience metrics may be based on adjustable load, reserve capacity and self-recovery time, which are shown in Table 6-1. The details of these metrics will be described in the next three paragraphs.

A commonly used expression “interruptible and curtailable loads”, which is defined by NERC as “use of interruptible and curtailable customer load to reduce capacity requirements or to conserve the fuel in short supply [71]” is synonymous to in adjustable load. This index may be used to reflect the effect of demand response, load shedding, under- frequency and under- voltage relays on load, frequency-sensitive load (i.e. motors). Based on the research done in demand response [72], [73], some load could be continuously modulated, but not cut off directly; thus the expression of “interruptible and curtailable load” is not preferred.

PJM classifies reserve as contingency/primary reserve and synchronized/spinning reserve, while NERC conclude spinning reserve as part of contingency reserve. NERC suggests that one of the requirement of contingency reserve is greater than the amount of reserve equal to the loss of the most severe single contingency or the amount of reserve equal to the sum of three percent of the load (generation minus station service minus Net Actual Interchange) and three percent of net generation (generation minus station service). PJM defines the Installed Reserve Margin (IRM) as the installed capacity percent above the forecasted peak load required to satisfy a Loss of Load Expectation (LOLE) of, on average, 1 Day/10 Years. Another important value defined by PJM is called Capacity Benefit Margin (CBM), expressed in megawatts, which is a single value that represents the simultaneous imports into PJM that can occur during peak PJM system conditions. PJM Staff recommends IRM as 15.5% for 2012/2013 delivery year, including 3500 MW CBM. Generally speaking, there are three types of reserve that may be defined for synchronous generators according to their response times, namely non-spinning reserve (with more than 5 minutes response time), spinning reserve (with almost 5 minutes response time), and regulator (frequency-based immediately response in milliseconds). Besides these three types of reserve, there are other types related to coupled load, generating and storage units and smart appliances responding to frequency, voltage variations.

Self-recovery time is the only index estimated from dynamic analysis. The previous two indices, namely adjustable load and reserve amount (at the exclusion of regulator), are estimated from static analysis. Self-recovery time may be included in our future work agenda if the scope of our research work is extended to include power system dynamic stability analysis.

Descriptive resilience metrics include ratio of the restoration time and or the amount of power outage or the number of affected customers of a power system with and without microgrids. The restoration process of a large-scale blackout after a hurricane usually starts with the restoration of the transmission network, then it is followed by the restoration of the distribution network, the critical load (hospital, bank and some research

institution, etc.), and finally the noncritical load. So the restoration time for critical load is taken account, as well as the time for noncritical load. For a common blackout where none of the components of the transmission system is physically damaged, the restoration phase begins with the restart of a first set of power plants, and then it is followed by their connection to a subsystem. Their power output is then ramped up while an equivalent amount of load is reconnected so that there is a balance between generation and load demand at every instant of time. This process is continued until all the power plants and loads are reconnected and the transmission system recovers its integrity.

Table 6-1 Proposed resilience metrics

	Resilience Metrics	
	Utility Grid's Resilience Metrics	End User's Resilience Metrics
Predictive	Adjustable Load; Reserve Amount & Response Time; Self-recovery Time;	Reserve Amount & Response Time; Adjustable Load;
Descriptive	Restoration Time; Power Outage/# of affected customers	Restoration Time; Cost for the utility outage

6.1.2 End User's Resilience Metrics

There are also predictive type and descriptive type of resilience metrics for end users. As the predictive resilience metrics for utility girds, reserve amount and adjustable load, which are shown in Table 6-1, are two indices that can be used as a metric for an end-user's resilience. Currently most regular end users do not have any reserve devices except hospitals, banks, some data centers and institutions which are willing to buy backup generators and storage devices. As smart grid and demand response develop, some residential households have been or will be provided with electrical vehicles or smart appliances such as micro-CHPs, HPs, smart controlled ACs, washers or dryers, which make it possible to modulate loads.

For example, some researchers on demand response set priorities to each controlled appliance, so that the total power consumption of a household suits several tolerance levels. Let us assume that a customer has several appliances with the priority from high to low as lightening, computer, AC, water heater which uses gas or electricity, or clothes dryer. As a first set of actions, the customer can only use lightening, computer, and AC which are running beyond a comfortable temperature range (setting temperature at $\pm 2°F$) due to certain strict demand limit. As a second set of actions, the customer can use lightening, computer, AC running within the comfortable range, clothes dryer, but not

water heater because water heater can work with gas. As a third set of actions, the customer is allowed to use any of his appliances, including water heater which could only consume electricity.

The descriptive metrics of end users also contain restoration time. In the last example about demand response, all restorations times according to different tolerance levels reflect the resilience of this customer. As for the critical loads like hospitals, there are restoration times with two tolerance levels, which are the duration time of a true blackout when even the backup generator and battery fail to run, and the duration time till the electricity from the system has been recovered.

Another descriptive index of end users is the cost for the utility outage. The purchase, maintenance and operation of backup generators and energy storage devices are costly. Even the residential customers under certain demand response strategy spend extra money, because the customer possibly has to consume extra gas to get some electricity during a utility outage.

6.2 Future Work

As it is shown in sub-section 5.5.2, the time average of system reserve capacity is calculated as one of the indices to evaluate the impacts of microgrid integration. The simulation results actually provide the system reserve capacity at each hour. However, the above data is not enough to obtain the resilience metrics that defined in the last section. The most critical missing part is the response times of the devices that are able to provide energy reserve. Within microgrids, energy storage devices like lithium-ion, lead-acid battery can give instant response; Renewable energy generators, which are typically connected to the main grid through invertors and convertors, are able to control in a flexible way their power exchange with the main grid in a very short time. Therefore, it is reasonable to think that microgrid penetration is likely to improve system resiliency. Due to the lack of actual information, we will leave this investigation as a future research work.

Although the computational burden of the sequential Monte Carlo simulations that applied the IS-AV method noticeably decreases in both case studies described in Section 5.5, the speed-up ratios of the current simulation are still remote from the requirement for an application in a large-scale power system. Therefore, as a future work, we will include the investigation on how to reduce the computational burden even further for large-scale systems.

References

[1] U.S.-Canada Power System Outage Task Force, Final report on the August 14, 2003 blackout in the United States and Canada: causes and recommendations, April 2004.

[2] IEEE PES CAMS Task Force on Understanding, Prediction, Mitigation and Restoration of Cascading Failures, Initial review of methods for cascading failure analysis in electric power transmission systems, IEEE Power Engineering Society General Meeting, Pittsburgh, PA USA July 2008.

[3] S. Chowdhury, S. P. Chowdhury, P. Crossley, "Microgrids and Active Distribution Networks", IET (UK), July 2009.

[4] R. Billinton, W. Li, Reliability assessment of electric power system using Monte Carlo methods, Plenum Press, New York, 1994.

[5] R. Y. Rubinstein, Simulation and the Monte Carlo method, John Wiley & Sons, Inc. New York, NY, USA, 1981

[6] R. Billinton, A. Jonnavithula, "Composite system adequacy assessment using sequential Monte Carlo simulation with variance reduction techniques," *IEE Proc.-Gener. Transm. Distrib.* Vol. 144, No. 1, pp 1-6, January 1997.

[7] L. Mili, Q. Qiu, A. G. Phadke, "Risk assessment of catastrophic failures in electric power systems," *International Journal of Critical Infrastructures*, Vol. 1, No. 1, pp. 38-63, 2004.

[8] J. De La Ree, Y. Liu, L. Mili, A. G. Phadke, L. Dasilva, "Catastrophic failures in power systems: Causes, analyses, and countermeasures," *Proceedings IEEE*, Vol. 93, No. 5, pp. 956-964, May 2005.

[9] J. S. Barrett, S. Dutta, O. Nigol, "A new computer model of ACSR conductors," *IEEE Trans. Power Apparatus and System*, Vol. PAS-102, No. 3, pp. 614-621, March 1983.

[10] S. L. Chen, W. Z. Black, M. L. Fancher, "High-temperature sag model for overhead conductors," *IEEE Trans. Power Delivery*, Vol. 18, No. 1, pp. 183-188, January 2003.

[11] J. F. Hall, A. K. Deb, "Prediction of overhead transmission line ampacity by stochastic and deterministic models," *IEEE. Trans. Power Delivery*, Vol. 3, No. 2, pp. 789-800, April 1988.

[12] I. Dobson, K. R. Wiezbicki, B. A. Carreras, V. E. Lynch, D. E. Newman, "An estimator of propagation of cascading failure," *39th Hawaii International Conference on System Sciences*, Kauai, Hawaii, January 2006.

[13] K. R. Wiezbicki, I. Dobson, "An approach to statistical estimation of cascading failure propagation in blackouts," *CRIS, Third International Conference on Critical Infrastructures*, Alexandria, Virginia, September 2006.

[14] J. S. Thorp, A. G. Phadke, S. H. Horowitz, S. Tamronglak, "Anatomy of Power System Disturbances: Importance Sampling," *Electrical Power and Energy Systems*, Vol. 20, No. 2, pp. 147-152, 1998.

[15] E. L. Davis, D. L. Funk, "Protective relay maintenance and application guide," *EPRI NP-7216 research project 2814-89 final report*, December 1993.

[16] X. Xiong, Y. Zhu, "Electrical sections of power plant (3rd edition)," *China Electric Power Press*, Beijing, 2004

[17] Reliability Test System Task Force. "IEEE reliability test system," *IEEE Trans. Power Apparatus and Systems*, Vol. PAS-98, No. 6, pp. 2047-2054, Nov./Dec. 1979.

[18] Reliability Test System Task Force. "The IEEE reliability test system – 1996," *IEEE Trans. Power Systems*, Vol. 14, No. 3, pp. 1010-1020, August 1999.

[19] http://www.weather.com/weather/climatology/USVA0265?climoMonth=7&cm_ven=USAToday&promo=0&site=www.usatoday.com&cm_ite=CityPage&par=usatoday&cm_cat=www.usatoday.com&cm_pla=WxPage.

[20] http://msdn.microsoft.com/en-us/library/system.random.aspx

[21] A. Sankarakrishnan, R. Billinton, "Sequential Monte Carlo Simulation Composite Power System Reliability Analysis with Time Varying Loads," *IEEE Trans. on Power Systems*, Vol. 10, No. 3, pp. 1540-1545, August 1995.

[22] C. Marnay, T. Strauss, "Effectiveness of antithetic sampling and stratified sampling in Monte Carlo chronological production cost modeling," *IEEE Trans on Power Systems*, Vol. 6, No. 2, pp 669-675, May 1991.

[23] L. Mili, "Taxonomy of the Characteristics of Power System Operating States", Proceedings of the Second RESIN workshop, Tucson, AZ, January 2011. http://www.nvc.vt.edu/lmili/docs/RESIN_Workshop_2011-White_Paper-Mili.pdf

[24] H. Clark, A. Edris, M. El-Gasseir, K. Epp, A. Isaacs, D. Woodford, "Softening the Blow of Disturbances – Segmentation with Grid Shock Absorbers for Reliability of Large Transmission Interconnections," *IEEE power & energy magazine*, pp. 30-41, Jan./Feb. 2008.

[25] R. C. Hardiman, M. T. Kumbale, Y. V. Makarov, "An advanced tool for analyzing multiple cascading failures," *8th International Conference on Probability Methods Applied to Power Systems*, pp. 629-634, Ames, IA, Septemper, 2004.

[26] D. S. Kirschen, D. Jayaweera, D. P. Nedic, R. N. Allan, "A Probabilistic indicator of system stress," *IEEE Trans on Power System*, Vol. 19, No. 3, pp 1650-1657, August 2004.

[27] M. Anghel, K. A. Werley, A. E. Motter, "Stochastic model for power grid dynamics," *Proccedings of the 40th Hawaii International Conference on System Sciences*, Waikoloa, HI, 2007.

[28] Z. Wang, A. Scaglione, R. J. Thomas, "A Markov-transition model for cascading failures in power grids," *45th Hawaii International Conference on System Sciences*, Maui, HI, 2012.

[29] S. S. Miller, "Extending traditional planning methods to evaluate the potential for cascading failures in electric power grids," *IEEE PES General Meeting*, Pittsburgh, PA, 2008.

[30] X. Yu, C. Singh, "A practical approach for integrated power system vulnerability analysis with protection failures," *IEEE Trans on Power Systems*, Vol. 19, No. 4, pp. 1811-1820, November 2004.

[31] C. Singh, A. D. Patton, "Protection system reliability modeling: unreadiness probability and mean duration of undetected faults," *IEEE Trans of Reliability*, Vol. R-29, No. 4, pp. 339-340, October 1980.

[32] K. Jiang, C. Singh, "New models and concepts for power system reliability evaluation including protection system failures," *IEEE Trans on Power Systems*, Vol. 26, No. 4, pp. 1845-1855, November 2011.

[33] C. Singh, J. Mitra, "Composite system reliability evaluation using state space pruning," *IEEE Trans on Power System*, Vol. 12, No. 1, pp. 471-478, February 1997.

[34] J. He, Y. Sun, D. S. Kirschen, C. Singh, L. Cheng, "State-space partitioning method for composite power system reliability assessment," *IET Gener. Transm. Distrib.*, Vol. 4, lss. 7, pp. 780-792, 2010.

[35] R. C. Green II, L. Wang, C. Singh, "State space pruning for power system reliability evaluation using genetic algorithms," *IEEE PES General Meeting*, Minneapolis, MN, July 2010.

[36] Y. Hou, C.-C. Liu, P. Zhang, K. Sun, "Constructing power system restoration strategies," *IEEE International Conference on Electrical and Electronics Engineering*, Bursa, 2009.

[37] N. Ozog, E. Desjardins, J. Jatskevich, "Bulk power system restoration interdependency risk modeling," *IEEE Electrical Power Conference*, Vancouver, BC, 2008.

[38] A. A. Mota, L. T. M. Mota, A. Morelato, "Simulation and analysis of restoration plans using fuzzy rule-based systems," *IEEE PES Transmission and Distribution Conference and Exposition: Latin America*, 2004.

[39] F. Ren, M. Zhang, D. Soetanto, X. Su, "Conceptual design of a multi-agent system for interconnected power systems restoration," *IEEE Trans on Power Systems*, Vol. 27, No. 2, May 2012.

[40] M. D. Stubna, J. Fowler, "An application of the highly optimized tolerance model to electrical blackouts," *International Journal of Bifurcation and Chaos*, Vol. 13, No. 1, 2003.

[41] B. A. Carreras, D.E. Newman, I. Dobson, A. B. Poole, "Initial evidence for self-organized criticality in electric power system blackouts," *Proceedings of 33rd Annual Hawaii International Conference on System Sciences*, January 2000.

[42] J. Chen, J. S. Thorp, I. Dobson, "Cascading dynamics and mitigation assessment in power system disturbances via a hidden failure model," *Electrical Power and Energy Systems*, Vol. 27, pp. 318-326, 2005.

[43] R. C. Hardiman, M. Kumbale, Y. V. Makarov, "Multi-scenario cascading failure analysis using TRELSS," *Quality and Security of Electric Power Delivery Systems, 2003. CIGRE/PES 2003. CIGRE/IEEE PES International Symposium*, October, 2003.

[44] A. Clauset, C. R. Shalizi, M. E. J. Newman, "Power-law distributions in empirical data," *SIAM Review 51(4), 661-703* (2009).

[45] S. Tamronglak, A. G. Phadke, S. H. Horowitz, J. S. Thorp, "Anatomy of Power System Blackouts: Preventive Relaying Strategies," *IEEE Trans. on Power Delivery*, Vol. 11, No.2, pp. 708-715, 1996.

[46] H. Wang, J. S. Thorp, "Optimal locations for protection system enhancement: A simulation of cascading outages," *IEEE Trans. Power Delivery*, Vol. 16, No. 4, pp. 528-533, October 2001.

[47] H. Hedyati, S.A. Nabaviniaki, A. Akbarimajd, "A Method for Placement of DG Units in Distribution Networks," *IEEE Trans. on Power Systems*, Vol. 23, No. 3, pp. 1620-1628, July 2008.

[48] Y. Yuan, K. Qian, C. Zhou, "The Optimal Location and Penetration Level of Distributed Generation," *Proceedings of the 42nd International Universities Power Engineering Conference*, Brighton, 2007.

[49] A. Arief, M. B. Nappu, A. Nizar, Z. Y. Dong, "Determination of DG Allocation with Modal Participation Factor to Enhance Voltage Stability," *Proceedings of the 8th International Conference on Advances in Power System Control, Operation and Management*, Hong Kong, China, 2009.

[50] M. F. AlHajri, M. R. A. AlRashidi, M.E. El-Hawary, "Improved Sequential Quadratic Programming Approach for Optimal Distribution Generation Sizing in

Distribution Networks," *Proceedings of the 23rd Canadian Conference on Electrical and Computer Engineering*, Calgary, AB, 2010.

[51] M. Gandomkar, M. Vakilian, M. Ehsan, "Optimal Distributed Generation Allocation in Distribution Network Using Hereford Ranch Algorithm," *Proceedings of the Eighth International Conference on Electrical Machines and Systems*, Volume 2, Nanjing, 2005.

[52] K. Nekooei, M. M. Farsangi, H. Nezamabadi-Pour, K. Y. Lee, "An Improved Multi-Objective Harmony Search for Optimal Placement of DGs in Distribution Systems," *IEEE Trans. on Smart Grid*, Vol. 4, No. 1, pp 557-567, March 2013.

[53] N. Kumar, P. Dutta, L. Xie, "Optimal DG Placement for Congestion Mitigation and Social Welfare Maximization," *Proceedings of the North American Power Symposium*, Boston, MA, 2011.

[54] M. R. Vallem, J. Mitra, S. B. Patra, "Distributed Generation Placement for Optimal Microgrid Architecture," *Proceedings of the IEEE PES Transmission and Distribution Conference and Exhibition*, Dallas, TX2006.

[55] A. K. Basu, A. Bhattacharya, S. P. Chowdhury, "Reliability Study of a Micro Grid System with Optimal Sizing and Placement of DER," *Proceedings of the IET-CIRED SmartGrids for Distribution*, Frankfurt, 2008.

[56] J. M. Gantz, S. M. Amin, A. M. Giacomoni, "Optimal Mix and Placement of Energy Storage Systems in Power Distribution Networks for Reduced Outage Costs," *Proceedings of the IEEE Energy Conversion Congress and Exposition*, Raleigh, NC, 2012.

[57] M. E. Khodayar, M. Barati, M. Shahidehpour, "Integration of High Rliability Distribution System in Microgrid Operation," *IEEE Trans. on Smart Grid*, Vol. 3, No. 4, pp 1997-2005, December 2012.

[58] P. Jahangiri, M. Fotuhi-Firuzabad, "Reliability Assessment of Distribution System with Distributed Generation," *Proceedings of the 2nd IEEE International Conference on Power and Energy*, Johor Bahru, 2008.

[59] M. Fotuhi-Firuzabad, A. Rajabi-Ghahnavie, "An Analytical Method to Consider DG Impacts on Distribution System Reliability," *Proceedings of the IEEE PES*

Transmission and Distribution Conference & Exhibition: Asia and Pacific, Dalian, 2005.

[60] I. Bae, J. Kim, "Reliability Evaluation of Customers in a Microgrid," *IEEE Trans. on Power Systems*, Vol. 23, No. 3, August 2008.

[61] S. Wang, Z. Li, L. Wu, M. Shahidehpour, Z. Li, "New Metrics for Assessing the Reliability and Economics of Microgrids in Distribution System," *IEEE Trans. on Power Systems*, Vol. 28, No. 3, August 2013.

[62] S. A. Arefifar, Y. A.-R. Mohamed, T. H. M. EL-Fouly, "Optimum Microgrid Design for Enhancing Reliability and Supply-Security," *IEEE Trans. on Smart Grid*, Vol. 4, No. 3, pp 1567-1575, September 2013.

[63] D. Menniti, A. Pinnarelli, N. Sorrentino, "A Method to Improve Microgrid Reliability by Optimal Sizing PV/Wind Plants and Storage Systems," *Proceedings of the 20th International Conference and Exhibition on Electricity Distribution*, Prague, Czech Republic, 2009.

[64] A. Navaeefard, S. M. M. Tafreshi, M. Barzegari, A. J. Shahrood, "Optimal Sizing of Distributed Energy Resources in Microgrid Considering Wind Energy Uncertainty with Respect to Reliability," *Proceedings of the IEEE International Energy Conference and Exhibition*, Manama, 2010.

[65] M. Braun, "Reactive Power Supplied by PV Inverters Cost Benefit Analysis," *Proceedings of the 22nd European Photovoltaic Solar Energy Conference and Exihibition*, Milan, Italy, September 2007.

[66] Q. Chen, L. Mili, "Composite Power System Vulnerability Evaluation to Cascading Failures Using Importance Sampling and Antithetic Variates", *IEEE Trans. Power Systems*, Vol. 28, No. 3, pp2321-2330, 2013.

[67] A. Nourai, "Distributed Bulk Storage: The future of batteries in grid applications," *Proceedings of the IEEE PES General Meeting*, San Diego, CA, 2011.

[68] A. T. Al-Awami, "Statistical Characterization of Wind Power Output for a Given Wind Power Forecast", *Proceedings of the North American Power Symposium*, Starkville, MS, 2009.

[69] A. Arulampalam, M. Barnes, A. Engler, A. Goodwin, N. Jenkins, "Control of Power Electronic Interfaces in Distributed Generation Microgrids", *INT. J. Electronics*, Vol. 91, No. 9, pp. 503-523, September 2004

[70] L. Mili, "Resilient and Sustainable Interdependent Electric Power and Communications Systems," Proceedings of the 3rd RESIN Workshop, Urbana-Champaign, Nov. 2011.

[71] North American Electric Reliability Corporation, Standard EOP-001-2b – Emergency Operations Planning, Nov. 4, 2010.

[72] S. Shao. *An approach of demand response for alleviating power system stree conditions due to electric vehicle penetration*. Ph.D. dissertation, Virginia Tech, Oct. 2011.

[73] F. Bliek, A. van den Noort, B. Roossien, R. Kamphuis, J. de Wit, J. van der Velde, M. Eijgelaar, "PowerMatching City, a living lab smart grid demonstration", *Proceedings of the IEEE PES conference ISGT Europe*, Gothenburg, Oct. 2010.

[74] NERC, Transmission Planning (TPL) Standards.
http://www.nerc.com/files/TPL-002-0.pdf;
http://www.nerc.com/files/TPL-003-0.pdf;
http://www.nerc.com/files/TPL-004-0.pdf.

[75] Y. Fu, Z. Li, "Different Models and Properties on LMP Calculations", *Proceedings of the IEEE PES General Meeting*, Montreal, Que, Jul. 2006.

[76] P. Kundur, Power System Stability and Control, McGraw Hill, Inc. New York, 1994.